Effect of CeO$_2$ and La$_2$O$_3$ promoters on Ni/Al$_2$O$_3$ oxygen carrier performance in chemical looping steam reforming of ethanol for hydrogen production

Miss Supalak Isarapakdeetham

A Thesis Submitted in Partial Fulfillment of the Requirements

for the Degree of Master of Engineering in Chemical Engineering

Department of Chemical Engineering

Faculty of Engineering

Chulalongkorn University

Academic Year 2018

ผลของตัวส่งเสริมชนิด CeO_2 และ La_2O_3 ต่อสมรรถนะของตัวนำพาออกซิเจนชนิด Ni/Al_2O_3 ในการปฏิรูปเอทานอลด้วยไอน้ำแบบเคมิคอลลูปปิงสำหรับการผลิตไฮโดรเจน

น.ส.ศุภลักษณ์ อิสระภักดีธรรม

จุฬาลงกรณ์มหาวิทยาลัย
CHULALONGKORN UNIVERSITY

วิทยานิพนธ์นี้เป็นส่วนหนึ่งของการศึกษาตามหลักสูตรปริญญาวิศวกรรมศาสตรมหาบัณฑิต
สาขาวิชาวิศวกรรมเคมี ภาควิชาวิศวกรรมเคมี
คณะวิศวกรรมศาสตร์ จุฬาลงกรณ์มหาวิทยาลัย
ปีการศึกษา 2561

Thesis Title   Effect of CeO_2 and La_2O_3 promoters on Ni/Al_2O_3 oxygen
                     carrier performance in chemical looping steam
                     reforming of ethanol for hydrogen production
By   Miss Supalak Isarapakdeetham
Field of Study   Chemical Engineering
Thesis Advisor   Professor Suttichai Assabumrungrat, Ph.D.
Thesis Co Advisor   Assistant Professor Pattaraporn Kim, Ph.D.

Accepted by the Faculty of Engineering, Chulalongkorn University in Partial Fulfillment of the Requirement for the Master of Engineering

<div style="text-align:right">Dean of the Faculty of Engineering</div>
(Professor SUPOT TEACHAVORASINSKUN, D.Eng.)

THESIS COMMITTEE

<div style="text-align:right">Chairman</div>
(Associate Professor Kasidit Nootong, Ph.D.)
<div style="text-align:right">Thesis Advisor</div>
(Professor Suttichai Assabumrungrat, Ph.D.)
<div style="text-align:right">Thesis Co-Advisor</div>
(Assistant Professor Pattaraporn Kim, Ph.D.)
<div style="text-align:right">Examiner</div>
(Rungthiwa Methaapanon, Ph.D.)
<div style="text-align:right">External Examiner</div>
(Assistant Professor Kanokwan Ngaosuwan, D.Eng.)

ศุภลักษณ์ อิสระภักดีธรรม : ผลของตัวส่งเสริมชนิด CeO_2 และ La_2O_3 ต่อสมรรถนะ ของตัวนำพาออกซิเจนชนิด Ni/Al_2O_3 ในการปฏิรูปเอทานอลด้วยไอน้ำแบบเคมิคอล ลูปปิงสำหรับการผลิตไฮโดรเจน. (Effect of CeO_2 and La_2O_3 promoters on Ni/Al_2O_3 oxygen carrier performance in chemical looping steam reforming of ethanol for hydrogen production) อ.ที่ปรึกษาหลัก : ศ. ดร.สุทธิชัย อัสสะบำรุง รัตน์, อ.ที่ปรึกษาร่วม : ผศ. ดร.ภัทรพร คิม

การศึกษาผลของ Ce และ/หรือ La ที่มีต่อ NiO/Al_2O_3 ในการปฏิรูปเอทานอลด้วยไอน้ำ แบบเคมิคอลลูปปิง ตัวนำพาออกซิเจนถูกเตรียมด้วยวิธีการอิมเพรกเนชันแบบเปียกและวิเคราะห์ คุณลักษณะด้วยวิธีต่างๆ ปฏิกิริยารีดอกซ์ทำการทดสอบที่อุณหภูมิ 500 องศาเซลเซียส โดยการ สลับสายป้อนระหว่างเชื้อเพลิง (FFS) และอากาศ (AFS) จากผลการทดสอบพบว่า Ce และ La ช่วยปรับปรุงคุณสมบัติของตัวนำพาออกซิเจนให้ดีขึ้นโดยปริมาณของ Ce และ La ที่เหมาะสมจะ ทำให้ตัวนำพาออกซิเจนมีความสามารถในการต้านทานการเกิดโค้กเพิ่มขึ้น ความสามารถในการ ละลายของ La ใน Ce ที่สังเคราะห์ได้มีค่า 50 เปอร์เซ็นโดยโมล โดยปริมาณของ La ที่เพิ่มขึ้นจะ ทำให้มี La_2O_3 กระจายตัวบนพื้นผิวของตัวนำพาออกซิเจนและดูดซับ CO_2 ในขั้นตอน FFS กลายเป็น $La_2O_2CO_3$ จากผลการทดสอบรอบที่ 1 พบว่าตัวนำพาออกซิเจน N/7LCA ให้ผลผลิต H_2 (3.2 โมลต่อโมลเอทานอลต่อนาที) มากที่สุด แต่เมื่อทำการทดสอบจนถึงรอบที่ 5 พบว่า N/3LCA มีเสถียรภาพที่ดี มีค่าการเปลี่ยนแปลงเอทานอล (88%) และผลผลิต H_2 (2.5) สูงที่สุดที่ เวลา 180 นาที โค้กที่มีลักษณะไม่แน่นอนที่สะสมบนตัวนำพาออกซิเจนสลายตัวในขั้นตอน AFS ที่ อุณหภูมิ 500 องศาเซลเซียส มีปริมาณน้อยลงเมื่อตัวนำพาออกซิเจนมีความเป็นเบสเพิ่มมากขึ้น ในส่วนของโค้กที่มีลักษณะเป็นเส้นใยและ $La_2O_2CO_3$ ไม่สามารถสลายตัวได้ที่อุณหภูมิ 500 องศา เซลเซียส จากการทดสอบปฏิกิริยารีดอกซ์หลายรอบพบว่าปริมาณของ La ที่มากเกินไปทำให้ตัวนำ พาออกซิเจนมีเสถียรภาพต่ำลง เนื่องจากการฟื้นฟู $La_2O_2CO_3$ ให้กลับมาเป็น La_2O_3 ต้องทำที่ อุณหภูมิสูง ซึ่งทำให้ความเสี่ยงของการหลอมรวมตัวของ Ni เพิ่มมากขึ้น

สาขาวิชา	วิศวกรรมเคมี	ลายมือชื่อนิสิต ....
ปีการศึกษา	2561	ลายมือชื่อ อ.ที่ปรึกษาหลัก ....
		ลายมือชื่อ อ.ที่ปรึกษาร่วม ....

5970461321 : MAJOR CHEMICAL ENGINEERING

Supalak Isarapakdeetham : Effect of CeO_2 and La_2O_3 promoters on Ni/Al_2O_3 oxygen carrier performance in chemical looping steam reforming of ethanol for hydrogen production. Advisor: Prof. Suttichai Assabumrungrat, Ph.D. Co-advisor: Asst. Prof. Pattaraporn Kim, Ph.D.

The effects of Ce and/or La on NiO/Al_2O_3 were studied in chemical looping steam reforming of ethanol. Oxygen carriers (OCs) were prepared by wet impregnation method and characterized by various techniques. The redox test was performed by alternating between fuel feed (FFS) and air feed step (AFS) at $500^{o}C$. It was found that Ce- and La-doped improved the OCs' properties. A suitable amount of Ce- and La-doping helped increase carbon tolerance due to oxygen storage capacity and mobility. The solubility limit was found at 50 mol% La in solid solution. At higher La-doping, La_2O_3 dispersed on the surface and adsorbed CO_2 to form $La_2O_2CO_3$ during the FFS. From the 1st cycle, N/7LCA displayed the highest H_2 yield (3.2 mol/mol ethanol-min). However, after the 5th cycle, N/3LCA exhibited more stability and presented the highest ethanol conversion (88%) and H_2 yield (2.5) at 180-min TOS, which decreasing from the 1st cycle 7% and 5%, respectively. Amorphous coke on the OCs decreased with increasing basicity and could be removed at $500^{o}C$ during AFS, while fibrous coke and $La_2O_2CO_3$ could not decompose at $500^{o}C$. Therefore, after multiple redox cycles, highly La-doped OCs exhibited rather low stability – suggesting that for La-doped OCs, higher regeneration temperature in AFS should be considered while Ni sintering at elevated temperature should be concerned.

Field of Study:	Chemical Engineering	Student's Signature ....
Academic Year:	2018	Advisor's Signature ....
		Co-advisor's Signature ....

ACKNOWLEDGEMENTS

จุฬาลงกรณ์มหาวิทยาลัย

CHULALONGKORN UNIVERSITY

TABLE OF CONTENTS

จุฬาลงกรณ์มหาวิทยาลัย
CHULALONGKORN UNIVERSITY

TABLE OF FIGURES

จุฬาลงกรณ์มหาวิทยาลัย
CHULALONGKORN UNIVERSITY

TABLE OF TABLES

จุฬาลงกรณ์มหาวิทยาลัย
CHULALONGKORN UNIVERSITY

CHAPTER I

INTRODUCTION

1.1 Introduction

Nowadays, global warming is one of the world's major problems which have drawn great attention from many countries. Greenhouse gases (e.g. CO_2, CH_4 and O_3) generated from human activities especially fossil fuel burning are the main cause of global warming. Since 2006, CO_2 concentration level (as shown in Fig. 1.1) has been increased from 380 ppm to 408 ppm. So, all sectors are cooperating to reduce energy consumption and to use more alternative energy such as solar power, wind power, biomass, tidal power, geothermal, etc. (http://www.altenergy.org/)
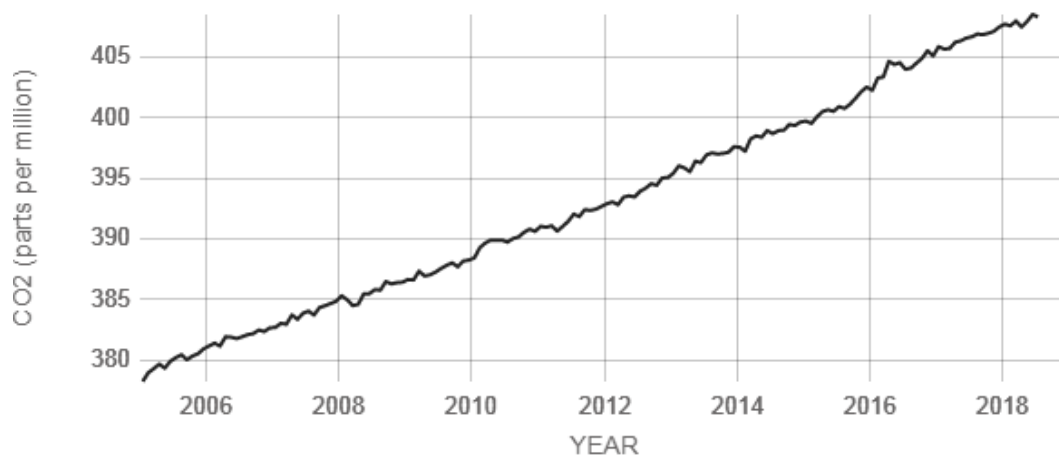
Figure 1.1 Global CO_2 emissions (https://climate.nasa.gov/)

Hydrogen has recently been given attention and proposed as one of the most desirable and efficient energy carriers instead of fossil fuels. It is often used as clean fuel in fuel cells because only water steam is produced in hydrogen combustion with very high energy release as shown in reaction (1) [1]. Moreover, hydrogen is used for the conversion of heavy petroleum fractions into lighters by hydrocracking process,

for the production of ammonia by Haber process, for the reduction of carbon monoxide to produce methanol. Hydrogen can be produced through different methods as shown in Fig. 1.2. The dominant route to produce hydrogen on a large scale from hydrocarbons or biomass is steam reforming [2-15] while other technologies such as sorption enhanced steam reforming [16, 17] with or without chemical looping process [18-24] from methane [8, 16, 18-21], methanol [6, 15], ethanol [4, 7, 9, 13, 14, 22-24], glycerol [5, 10-12], acetic acid [2, 3] have been proposed. Among the hydrocarbons and oxygenated compounds, ethanol is considered as an important candidate because of high H content, less hazard, safe transport and high heating value, and it can be produced economically and sustainably in large amounts from biomass such as agricultural wastes [25, 26].

$$H_2(g) + 1/2 O_2(g) \rightarrow H_2O(g) \qquad \Delta H_{298\ K} = -241.81 \text{ kJ/mol} \qquad (1)$$
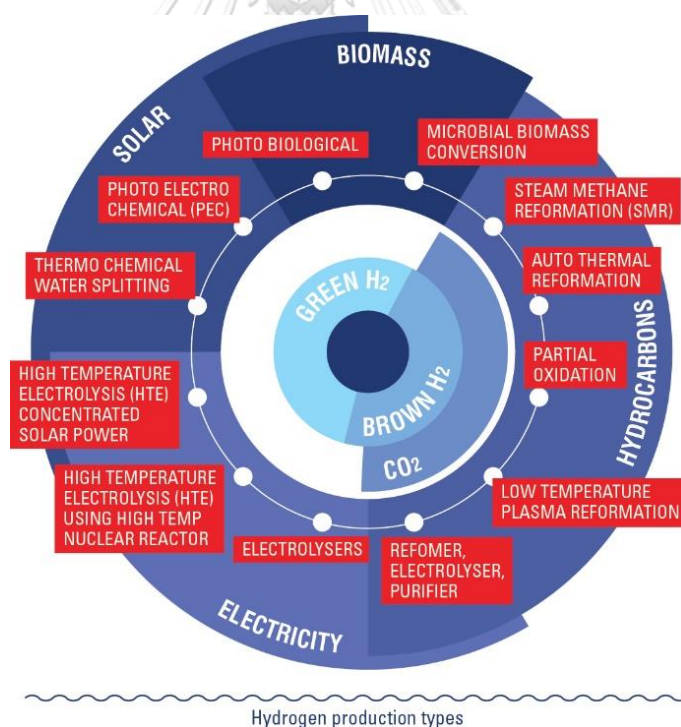
Figure 1.2 Hydrogen production methods

(http://www.hydroville.be/en/waterstof/hoe-maak-je-waterstof/)

Although carbon dioxide is produced from steam reforming of ethanol (reaction (7)), it can be captured for hydrogen purification by CO_2 adsorbent such as calcium oxide (CaO) and be separated from the carbonate at high temperatures by reactions (2) and (3), respectively and be stored at deep underground or deep inside sea storage (Fig. 1.3) [27] with no CO_2 emission.

$$CaO(s) + CO_2(g) \rightarrow CaCO_3(s) \qquad \Delta H_{298\,K} = -175.7 \text{ kJ/mol} \qquad (2)$$

$$CaCO_3(s) \rightarrow CaO(s) + CO_2(g) \qquad \Delta H_{298\,K} = 175.7 \text{ kJ/mol} \qquad (3)$$
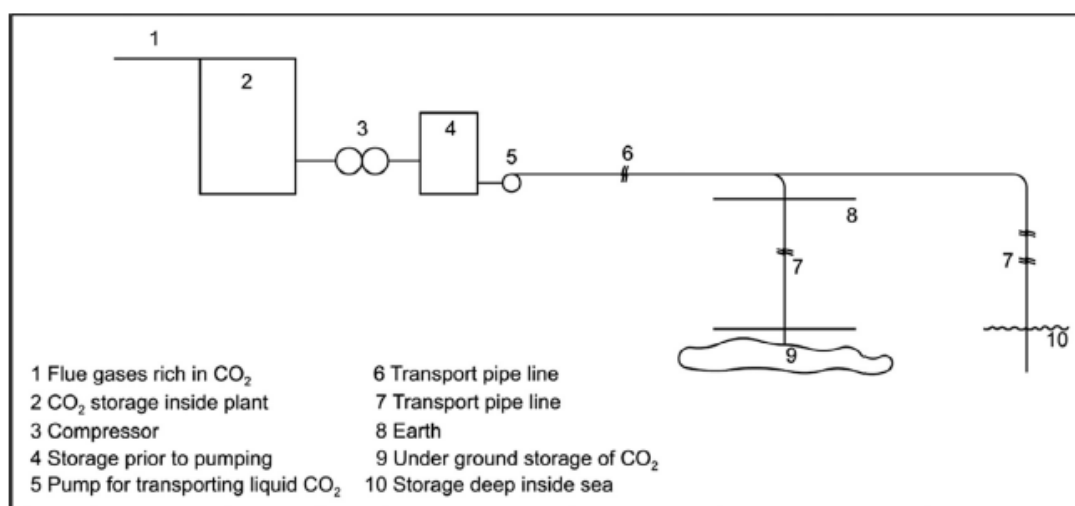
Figure 1.3 Flow-chart for CO_2 collection, compression, transport, and storage [27]

There are two groups of metal which are often used as catalysts for steam reforming of ethanol, consisting of noble metals (Rh, Pt, Pd, Ru, Ir) and transition metals (Ni, Co, Cu, Fe). In case of noble metals, there are many advantages for steam reforming comprising of good catalytic activity and resistance to carbon formation except their high cost and low availability [28]. Among the transition metals, Ni is the best catalyst for hydrogen production by steam reforming which shows more than 90% hydrogen selectivity [29]. However, Ni-based catalysts generally suffer rapid deactivation caused by sintering of active nickel species and carbon deposition, which remains a major challenge for developing Ni-based catalysts [30], [31]. An

effective way of improving Ni dispersion and suppressing the aggregation of Ni nanoparticles is spreading them on porous supports [32]. Alumina is often used as support because of its high surface area but the Lewis acid sites of the alumina cause carbon deposition due to ethylene production [29], [33]. To adjust the stability of alumina supported Ni, rare earth metals are promoted on the catalysts to reduce acidity, reduce Ni particle size and improve Ni dispersion [34].

Chemical looping steam reforming refers to the reduction and oxidation of oxygen carriers (OCs) which are circulated between a fuel reactor (FR) and an air reactor (AR). An oxygen carrier, often metal oxide, is used to transfer the oxygen from the air to the fuel between two reactors. The reduced oxygen carrier is then recycled by using air to oxidize the carrier to its original state. It should be noted that reduced oxygen carrier also acts as a reforming catalyst. The oxidation reaction of oxygen carriers is very exothermic and the reduction reaction is endothermic so this process acts as auto-thermal condition which reduces the external energy consumption [22]. Moreover, carbon deposition on catalyst can be eliminated during the process of oxygen carriers regeneration, this process utilizes air rather than pure oxygen from costly air separation process and achieves heat balance in auto-thermal condition [25].

Metal oxides of Fe, Ni, Co, Cu, Mn and Cd have been studied, mostly for chemical looping of gaseous fuels such as natural gas or methane [20, 35, 36]. Chemical looping of liquid fuels such as ethanol has also been reported [22, 23, 37]. Metal oxide of Ni is relatively low cost and was found to provide a high oxidation/reduction rate which is suitable for chemical looping process [25, 38]. Zafar et al. have studied Ni, Cu, Fe and Mn supported on SiO_2 or $MgAl_2O_4$ as oxygen carriers and the results showed that Ni-based oxygen carriers are the most feasible for chemical looping process [35]. However, Ni is still susceptible to agglomeration and carbon deposition during the reforming process.

For agglomeration problem, the impregnation of oxygen carriers onto substrates was found to reduce agglomeration and increase the reactivity of the oxygen carriers [25]. The different types of alumina support were reported to affect the reactivity of the oxygen carriers and on the gas product distribution. De Diego et al. reported that the reduction reactivity of the NiO/α-Al_2O_3 was higher than NiO/γ-Al_2O_3 because of the limited solid state reaction between NiO and α-Al_2O_3 [39].

For carbon deposition problem, the usage of proper oxygen carriers with high oxygen storage capacity (OSC) and high mobility (OM) was found to reduce carbon deposition on the oxygen carriers. Jiang et al. studied various oxygen carriers and found that oxygen carriers with high OSC and OM could reduce carbon deposition during hydrogen production process due to the oxygen lattice diffusion to oxidize the carbon formation [40]. Therefore, the excellent oxygen carriers should perform as high reactivity, high OSC, high OM, high resistance to sintering and high stability [41].

Rare earths (Ce, La) have been widely used as a promoter doped on catalysts in reforming process to improve the metal dispersion and metal-support interaction [9, 33, 42, 43]. Ceria (CeO_{2-x}) exists in a fluorite structure, which is favorable for the diffusion of oxygen lattice and oxygen vacancy formation. Therefore, ceria exhibits high OSC and OM since it easily releases, stores and transports oxygen [44]. Moreover, in reforming process, CeO_2 can promote the water gas shift (WGS) reaction and also prevent the sintering of metallic species [45, 46]. In Ni-ceria/NiO-ceria chemical looping, ceria can also act as an oxygen carrier due to its high OSC and OM properties. In this work, La^{3+} aliovalent dopant (La_2O_3) was used to enhance OSC and OM of ceria as well as to reduce carbon deposition on the Ni catalyst. It should be importantly noted that La_2O_3 addition was reported to help reducing carbon deposition on catalyst in reforming process [33] since La_2O_3 can adsorb and react with CO_2 to form lanthanum oxy-carbonate species act as a carbon reservoir (reaction (4)) [23, 47-50]. Therefore, La_2O_3 can act as CO_2 sorption in the process. The addition of La_2O_3 is also expected to reduce the surface acidity of Al_2O_3 support.

Although lanthanum doped ceria has been employed extensively as a reforming catalyst, up to date the effect of ceria doping as an oxygen carrier on the redox property and stability has not been of much attention in the chemical looping process.

$$La_2O_3(s) + CO_2(g) \rightarrow La_2O_2CO_3(s) \tag{4}$$

The aim of this study is to study the effect of addition CeO_2 and/or La_2O_3 as a promoter on Ni-based oxygen carriers performance for chemical looping steam reforming of ethanol. It is expected that CeO_2 and/or La_2O_3 incorporation ought to improve the Ni dispersion, enhance reducibility of NiO which shortened the dead time in the fuel feed step, improve the efficiency of hydrogen production and reduce carbon deposition due to carbon gasification during the fuel feed step. In case of La_2O_3, the formed $La_2O_2CO_3$ should provide the higher hydrogen purity in the effluent gas. The role of lanthanum doped ceria as an oxygen carrier in corporate with Ni metal as well as the role of material in reducing carbon deposition is of interest.

1.2 Objective

To study effect of the addition of CeO_2, La_2O_3 and CeO_2-La_2O_3 on Ni/Al_2O_3 oxygen carrier on hydrogen production in chemical looping steam reforming of ethanol.

1.3 The scope of research

1) Various weight ratio of rare earth oxides (CeO_2 : La_2O_3 are 0 : 10, 1 : 9, 3 : 7, 5 : 5, 7 : 3, 9 : 1 and 10 : 0) were promoted on 12.5wt.%Ni/Al_2O_3 oxygen carriers by wet impregnation method to determine the activity of oxygen carriers for chemical looping steam reforming of ethanol.

2) The oxygen carriers were characterized by N_2 adsorption-desorption, XRD, H_2-TPR, CO_2-TPD, SEM-EDX and TGA to determine their physical and chemical properties.

3) The activity tests and stability tests with 5 cycles of oxygen carriers were carried out by chemical looping steam reforming of ethanol at atmospheric pressure.

4) Fuel feed step referred to fuel reforming as well as the reduction reaction of oxygen carriers while air feed step referred to oxidation reaction of a reduced oxygen carrier to oxidize the carrier to its original state.

5) Post analysis is performed. The used oxygen carriers were characterized by XRD, SEM-EDX and TGA to determine the change in properties and carbon deposition.

1.4 Research methodology

1) Doping CeO_2 and La_2O_3 on Al_2O_3 via wet impregnation method and calcined at 650°C for 6 h to obtain CeO_2-Al_2O_3, La_2O_3-Al_2O_3 and La_2O_3-CeO_2-Al_2O_3.

2) Loading Ni on Al_2O_3, CeO_2-Al_2O_3, La_2O_3-Al_2O_3 and La_2O_3-CeO_2-Al_2O_3 via wet impregnation method and calcined at 500°C for 4 h to obtain Ni/Al_2O_3, Ni/CeO_2-Al_2O_3, Ni/La_2O_3-Al_2O_3 and Ni/La_2O_3-CeO_2-Al_2O_3 as oxygen carriers.

3) Investigation the performance of each oxygen carriers in chemical looping steam reforming of ethanol at various operation condition at atmospheric pressure.

4) Characterization of fresh oxygen carriers, used oxygen carriers by XRD, N_2 adsorption-desorption, H_2-TPR, CO_2-TPD, SEM-EDX and TGA/DSC.

CHAPTER II
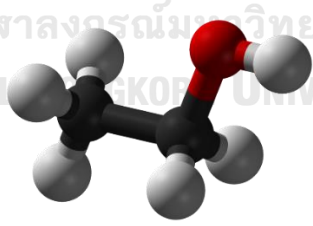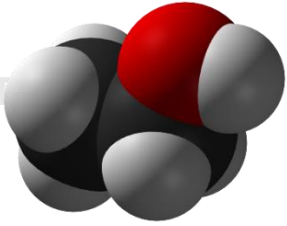
BACKGROUND AND LITERATURE REVIEWS

2.1 Ethanol

Ethanol (also called ethyl alcohol) is a volatile, flammable, clear colorless liquid with a slight characteristic odor. It is naturally produced by fermentation of sugars by yeasts or via petrochemical processes. This compound is widely used as a chemical solvent, either for scientific chemical testing or in synthesis of other organic compounds, and is a vital substance utilized across many different kinds of manufacturing industries. Ethanol is also used as a clean-burning fuel source (http://www.chemicalsafetyfacts.org/). Some properties of ethanol are shown in Table 2.1.

Table 2.1 Structure and properties of ethanol molecule.
(https://pubchem.ncbi.nlm.nih.gov/)

Molecular formula	C_2H_5OH
Structure	
Molar mass	46.069 g/mol
Appearance	clear colorless liquid with a slight characteristic odor
Density	789 kg/m^3 (at 20°C)
Melting point	-114.1°C
Boiling point	78.2°C
Solubility in water	1,000,000 mg/L (at 25°C)
Heating value	26.952 – 29.847 MJ/kg (from ESSOM CO.,LTD, Thailand)

2.2 Steam reforming process (SR)

The steam reforming process is the most widely employed route for hydrogen which is consists of steam reforming reaction and water gas shift reaction as shown in reactions (5) and (6), respectively. There are two groups of fuels using in steam reforming system consist of light hydrocarbon (refinery gases, LPG, natural gas, naphtha) and heavy hydrocarbon (oil, tar, asphalt, petroleum coke, coal). Hydrogen production via steam reforming process is divided into 3 steps as shown in Fig. 2.1. Firstly, fuels are fed into the reformer with steam at high temperature and pressure due to highly endothermic reaction. The effluent gas from reformer is sent to the water gas shift reactor includes high temperature shift reactor (HTS) and low temperature shift reactor (LTS) to convert carbon monoxide into more hydrogen. Lastly, hydrogen is separated by a purification unit to obtain more than 95% purity of hydrogen. The advantage of steam reforming process is the high efficiency and low production costs. [51]

$$CH_4(g) + H_2O(g) \leftrightarrow 3H_2(g) + CO(g) \qquad \Delta H_{298\ K} = 206\ kJ/mol \qquad (5)$$

$$CO(g) + H_2O(g) \leftrightarrow H_2(g) + CO_2(g) \qquad \Delta H_{298\ K} = -41\ kJ/mol \qquad (6)$$
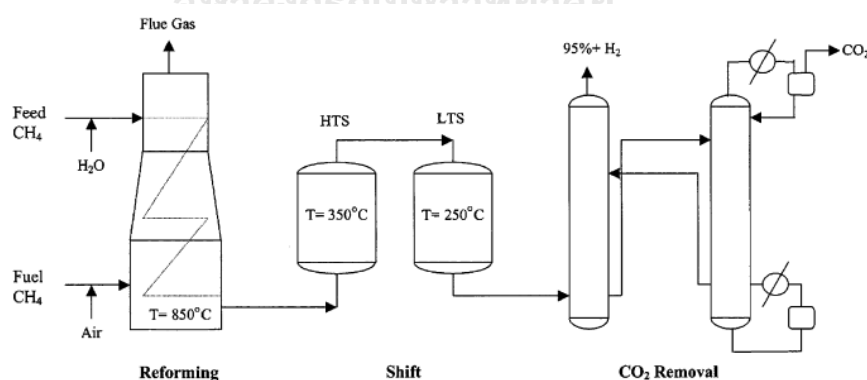
Figure 2.1 Flow-sheet for a conventional steam reforming for hydrogen production [52]

Ethanol is interesting source of hydrogen because it can be obtained from renewable biomass (e.g. sugar cane). Its advantage is also low toxic and safety handling. The overall ethanol steam reforming reaction are shown in reaction (7). However, there are several other reactions which generate unwanted products by ethanol dehydrogenation (reaction (8)), ethanol decomposition (reaction (9)), ethanol dehydration (reaction (10)), ethanol dehydrogenolysis (reaction (11)), acetaldehyde decomposition (reaction (12)), Boudouard reaction and other intermediate reactions for the carbon deposition on the catalyst surface (reactions (13) – (17)). [28] These reactions can be written in pathway as shown in Fig. 2.2.

$$C_2H_5OH(g) + 3H_2O(g) \rightarrow 2CO_2(g) + 6H_2(g) \qquad \Delta H_{298\,K} = 347.4 \text{ kJ/mol} \qquad (7)$$

$$C_2H_5OH\,(g) \leftrightarrow CH_3CHO(g) + H_2(g) \qquad \Delta H_{298\,K} = 68.5 \text{ kJ/mol} \qquad (8)$$

$$C_2H_5OH\,(g) \leftrightarrow CH_4(g) + CO(g) + H_2(g) \qquad \Delta H_{298\,K} = 49.6 \text{ kJ/mol} \qquad (9)$$

$$C_2H_5OH\,(g) \leftrightarrow C_2H_4(g) + H_2O(g) \qquad \Delta H_{298\,K} = 45.4 \text{ kJ/mol} \qquad (10)$$

$$C_2H_5OH\,(g) + 2H_2(g) \rightarrow 2CH_4(g) + H_2O(g) \qquad \Delta H_{298\,K} = -156.2 \text{ kJ/mol} \qquad (11)$$

$$CH_3CHO(g) \leftrightarrow CH_4(g) + CO(g) \qquad \Delta H_{298\,K} = -18.9 \text{ kJ/mol} \qquad (12)$$

$$C_2H_4(g) \rightarrow 2C(s) + H_2(g) \qquad \Delta H_{298\,K} = -52.4 \text{ kJ/mol} \qquad (13)$$

$$CH_4(g) \leftrightarrow 2H_2(g) + C(s) \qquad \Delta H_{298\,K} = 75 \text{ kJ/mol} \qquad (14)$$

$$2CO(g) \leftrightarrow CO_2(g) + C(s) \qquad \Delta H_{298\,K} = -172 \text{ kJ/mol} \qquad (15)$$

$$CO(g) + H_2(g) \leftrightarrow H_2O(g) + C(s) \qquad \Delta H_{298\,K} = -131 \text{ kJ/mol} \qquad (16)$$

$$CO_2(g) + 2H_2(g) \leftrightarrow 2H_2O(g) + C(s) \qquad \Delta H_{298\,K} = 306 \text{ kJ/mol} \qquad (17)$$

Figure 2.2 Reactions pathway in the ethanol steam reforming [29]

2.3 Chemical looping reforming method

In the chemical looping steam reforming, metal oxide is used as oxygen carriers which are reduced and oxidized in a cyclic manner. It is usually performed in two reactors which are fuel reactor (FR) and air reactor (AR) to reduce and oxidize the oxygen carriers, respectively. In the fuel feed step, fuel is oxidized by lattice oxygen from the oxygen carriers into synthesis gas, which is convert to be H_2 by WGS reaction, while metal oxide is (MeO) reduced into metal (Me) and Me_yO_{x-1} (reaction (18)). The initial period in the fuel reactor also called 'dead time' because of no H_2 generation, and this 'dead time' is the indicator of the reducibility of oxygen carriers. When the MeO sufficiently convert to Me, steam reforming to syngas and WGS occur (reaction (19) and (6)). Then in the air feed step, the reduced oxygen carriers (Me) is transferred to air reactor for replenishment of oxygen from air to be MeO and to combust the carbon deposition on oxygen carriers as shown in reactions (20) and (21). The reactions in the fuel reactor and air reactor are endothermic and exothermic, respectively, so the overall reactions are achieved auto-thermal

conditions. [23, 25, 26, 53] The diagram of chemical looping reforming method is shown in Fig. 2.3.

$$C_2H_5OH(g) + 6MeO(s) \rightarrow 2CO_2(g) + 3H_2O(g) + 6Me(s)$$

$$\text{or } C_2H_5OH(g) + Me_yO_x(s) \rightarrow 2CO(g) + 3H_2(g) + Me_yO_{x-1}(s) \qquad \Delta H_{298\ K} > 0 \qquad (18)$$

$$C_2H_5OH(g) + H_2O(g) \rightarrow 2CO(g) + 4H_2(g) \qquad \Delta H_{298\ K} = 256\ kJ/mol \quad (19)$$

$$2Me(s) + O_2(g) \rightarrow 2MeO(s)$$

$$\text{or } 2Me_yO_{x-1}(s) + O_2(g) \rightarrow 2Me_yO_x(s) \qquad \Delta H_{298\ K} < 0 \qquad (20)$$

$$C(s) + O_2(g) \rightarrow CO_2(g) \qquad \Delta H_{298\ K} = -394\ kJ/mol \quad (21)$$
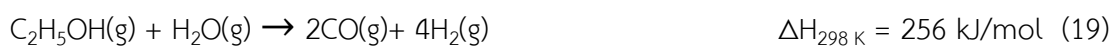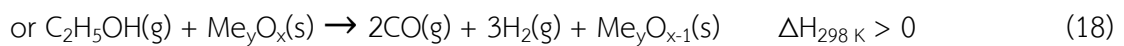
Figure 2.3 Working principle of chemical looping reforming [24]

For the fixed bed reactor, chemical looping reforming is performed by switching the feed gas between fuel feed and air feed. Adanez et al. [41] have proposed that the excellent oxygen carriers should fulfill several characteristics such as high oxygen mobility (OM), high resistance to sintering, high catalytic reactivity and limited cost.

2.4 Materials for steam reforming reaction and chemical looping reforming system

Mattisson et al. [35] studied different transition state metal oxides as the active phase of oxygen carriers such as Ni, Cu, Fe and Mn supported on SiO_2 and $MgAl_2O_4$ in the two interconnected fluidized beds, and the results conclude that Ni-based particles are most feasible oxygen carriers for both chemical looping combustion (CLC) and CLR. In spite of the excellent reactivity of Ni-based oxygen carriers, the main obstacles for the application are the rapid deactivation from meta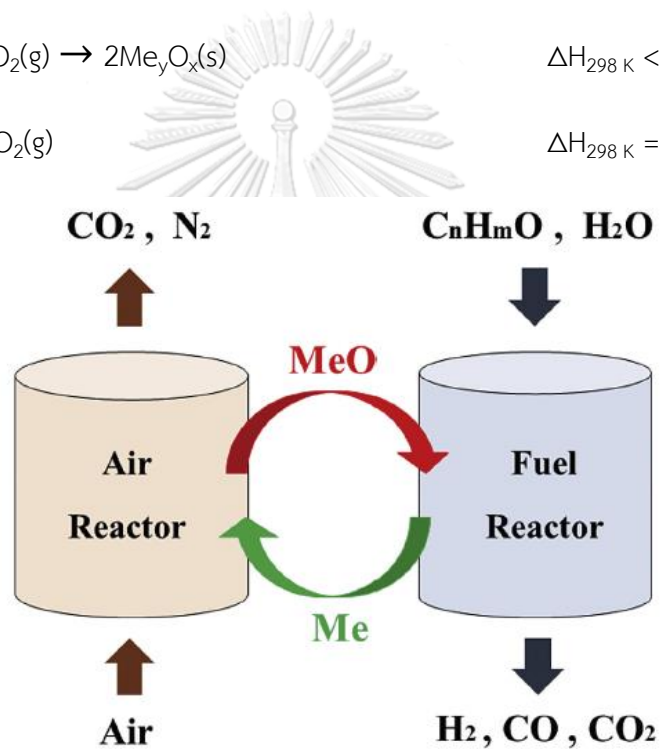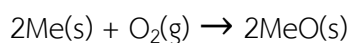l sintering due to the low Tamman temperature and insufficient oxygen mobility because of the high activation energy (2.23 eV in CLR) of oxygen anion diffusion of NiO [54]. The conversion of oxygenates are increased when increase amount of active Ni metal. 10-15 wt% is reported as the optimum Ni loading, however, the increased amount of Ni loading may affect to sintering [55].

Al_2O_3 is often used as inert support because of their high mechanical resistance, proper chemical stability and high melting point. The Al_2O_3 support increases the porosity, surface area and dispersion of metal loading and improves the reactivity. Karimi et al. [36] prepared oxygen carriers by precipitation method using inert materials Al_2O_3 and TiO_2 as supports for chemical looping reforming system in fixed bed reactor at high temperature (700–1200°C). The results showed that the better reactivity of Al_2O_3 compared to TiO_2 because of more porous structure and higher surface area for chemical looping reforming process. However, the acidic properties of Al_2O_3 are caused the carbon deposition [36]. The acidity and basicity of the support are affected to metal particle size and metal-support interaction [50]. The support with basicity properties or adding basic promoters on the catalyst surface proposes and increase of adsorbed oxygen atoms (O_{ad}) [56]. It is well known that ceria-promoted materials are suppressed the carbon deposition on the active phase due to the properties of CeO_2: high reducibility, oxygen mobility, oxygen storage capacity [57]. The CeO_2 concentration influences on the metal-support

interaction, the dispersion of the active metal sites and carbon removal [50]. La_2O_3 is usually used as promoters because La_2O_3 can improve the properties of catalyst such as basicity properties of the supports and metal-support interaction [56]. Montero et al. [58] studied ethanol steam reforming by using Ni supported on La_2O_3-Al_2O_3 and reported that La_2O_3 can suppress the formation of ethylene which is coke precursor. In addition, La_2O_3 can react with CO_2 to form $La_2O_2CO_3$ which improve the catalyst activity and stability [56, 59, 60].

จุฬาลงกรณ์มหาวิทยาลัย
CHULALONGKORN UNIVERSITY

Table 2.2 Summary of previous works with different catalysts, supports and conditions for steam reforming reaction and chemical looping reforming system

Catalyst	Reaction	Amount (g)	Temperature (°C)	S/E mol ratio	Ethanol conversion (%)	H_2 yield (mol/mol ethanol)	Ref.
5%Co/calcium hydroxyapatite	SR	0.15	500	6	41-67	1.5	[4]
5.5%Ni/Ce-Al-Mg	SR	3.00	540	3	87	4.0	[9]
6%Ni/SBA-15	SR	0.20	550	3	100	5.1	[13]
7%Ni/CeO_2-MgO	SR	0.03	600	6	100	4.2	[14]
12%Ni/MMT-TiO_2	SR	0.50	500	10	84	3.3	[61]
15%Ni/Sr-Al_2O_3-ZrO_2	SR	0.10	450	6	100	2.6	[34]
7.5%Ni-7.5%Co/Al_2O_3	SR	0.50	550	13	97	N/A	[62]
14%Ni/Al_2O_3	SR	0.10	450	6	100	1.4	[63]
15%Ni/ZnO-Al_2O_3	SR	0.02	500	3	100	N/A	[64]
$NiMn_2O_4$	CLR	1.00	600	3	N/A	3.3	[22]
$LaNiO_3$-Ca	CLR	0.50	600	6	86	3.7	[23]
$LaNiO_3$/MMT	CLR	0.50	650	6	90	4.2	[24]

CHAPTER III

EXPERIMENTAL

3.1 Chemicals and gases

1. Alumina (Al_2O_3, Sigma Aldrich)

2. Nickel nitrate hexahydrate ($Ni(NO_3)_2.6H_2O$, Sigma Aldrich)

3. Lanthanum nitrate hexahydrate ($La(NO_3)_3.6H_2O$, Sigma Aldrich)

4. Cerium nitrate hexahydrate ($Ce(NO_3)_3.6H_2O$, Sigma Aldrich)

5. Nitrogen gas, 99.999% purity (N_2, Linde)

6. Oxygen gas, 99.999% purity (O_2, Linde)

7. Hydrogen gas, 99.999% purity (H_2, Linde)

8. Argon gas, 99.999% purity (Ar, Linde)

9. Helium gas, 99.999% purity (He, Linde)

10. Deionized water

3.2 Preparation of oxygen carriers

The oxygen carriers were prepared by wet impregnation method. Alpha-alumina and mixed aqueous solution of cerium nitrate hexahydrate ($Ce(NO_3)_3.6H_2O$) and lanthanum nitrate hexahydrate ($La(NO_3)_3.6H_2O$) were stirred at the temperature of 70°C until the solution transforming to slurry. Then, the supports were dried at 110°C overnight and calcined at 650°C for 6 hours under stagnant air. Supported Ni oxygen carriers were prepared by wet impregnation method using an aqueous solution of nickel nitrate hexahydrate ($Ni(NO_3)_2.6H_2O$) and using similar procedure as mentioned above but calcined at 500°C for 4 hours. The Ni and mixed rare earth

oxides content were fixed at 12.5wt.% and 10wt.%, respectively, corresponding to 12.5wt% Ni with lanthana and ceria doped alumina (12.5wt%Ni/$x$wt%La$_2$O$_3$-(10-x)wt%CeO$_2$-Al$_2$O$_3$). These samples were labeled as N/A, N/CA, N/LA and N/xLCA where N=Ni, C=CeO$_2$, L=La$_2$O$_3$, A=Al$_2$O$_3$ and x represented as weight percent of lanthana in oxygen carriers. Figure 3.1 shows the synthesis steps of oxygen carriers.
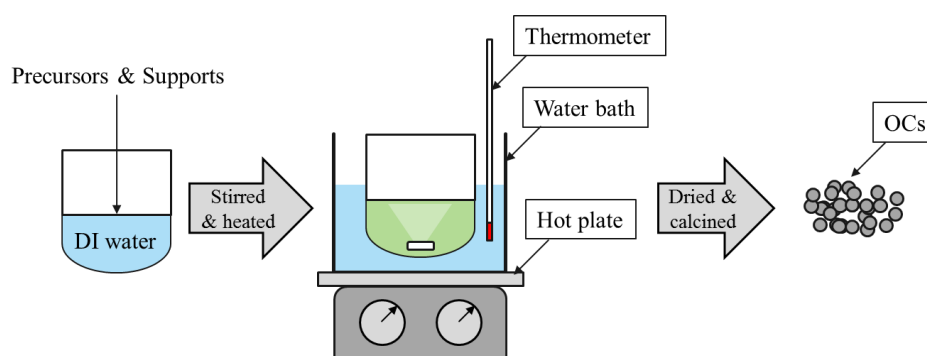
Figure 3.1 Steps of oxygen carrier synthesis by wet impregnation method

3.3 Oxygen carrier characterization

3.3.1 X-ray diffraction (XRD)

The XRD patterns were analyzed by Bruker D8 Advance, using a Cu Kα radiation as x-ray source at a wavelength of 0.154056 nm. The patterns were recorded over Bragg angles between 20° and 80° with a step size of 0.04° and scan speed of 0.5. The crystallite size of the metal was calculated using the Scherrer's equation.

3.3.2 N$_2$ adsorption-desorption

The Brunauer-Emmet-Teller (BET) method was performed with liquid nitrogen at -196°C on a Micromeritics ASAP 2020 instrument. All samples were degassed before the test under vacuum for 12h at 200°C. The surface area measurement was based on the BET method, and the pore volume and pore size were calculated by the BJH method.

3.3.3 H_2-temperature programmed reduction (H_2-TPR)

H_2-TPR experiments were carried out to determine the strength of the metal-support interaction of the oxygen carriers. Each oxygen carriers (0.1 g) were packed into a quartz tube reactor and were pretreated under nitrogen flow (25 ml/min) at 250°C for an hour to remove humidity and contaminates. Then, the sample was heated from room temperature to 800°C at a rate of 10°C/min in 10%H_2 in Ar. The hydrogen consumption was recorded by thermal conductively detector (TCD) and the water produced in TPR was trapped by a cold trap.

3.3.4 CO_2-temperature programmed desorption (CO_2-TPD)

The basicity on oxygen carriers was determined by CO_2-TPD. Each oxygen carriers (0.1 g) were packed into a quartz tube reactor and were pretreated under helium flow (25 ml/min) at 250°C for an hour before cooling down to 50°C. After that, 25 ml/min of CO_2 was introduced to the reactor for 30 min. The CO_2-saturated oxygen carrier was purged by He until baseline was stable. The TPD profile was recorded with TCD (Micromeritics 2750) with a heating rate of 10°C/min.

3.3.5 Scanning electron microscope/Energy dispersive x-ray spectroscopy (SEM/EDX)

The morphology and the elemental distribution on a surface of the catalysts was investigated by SEM/EDX (Hitachi S-3400N/EDAX Apollo X) using Link Isis series 300 program SEM (JEOL model JSM-5800LV).

3.3.6 Thermogravimetry analysis/Differential scanning calorimeter (TGA/DSC)

TGA/DSC was carried out under air flow from room temperature to 1000°C at a rate of 10°C/min to calculate the amount of carbon deposition on the used sample. The technique was also used for comparing the oxidation degree and the oxidation rate in the oxidation half cycle in the fuel feed step.

3.4 Chemical looping steam reforming of ethanol

The oxygen carriers (0.5 g) supported by quartz wool were loaded into a quartz fixed bed reactor (∅16 x 500 mm) to perform chemical looping steam reforming of ethanol, equipped with a coaxial thermocouple for temperature monitoring and controlling. The reactor was heated electrically using a tubular furnace to a set temperature of 500°C. The schematic diagram of the laboratory system is shown in Fig. 3.2.
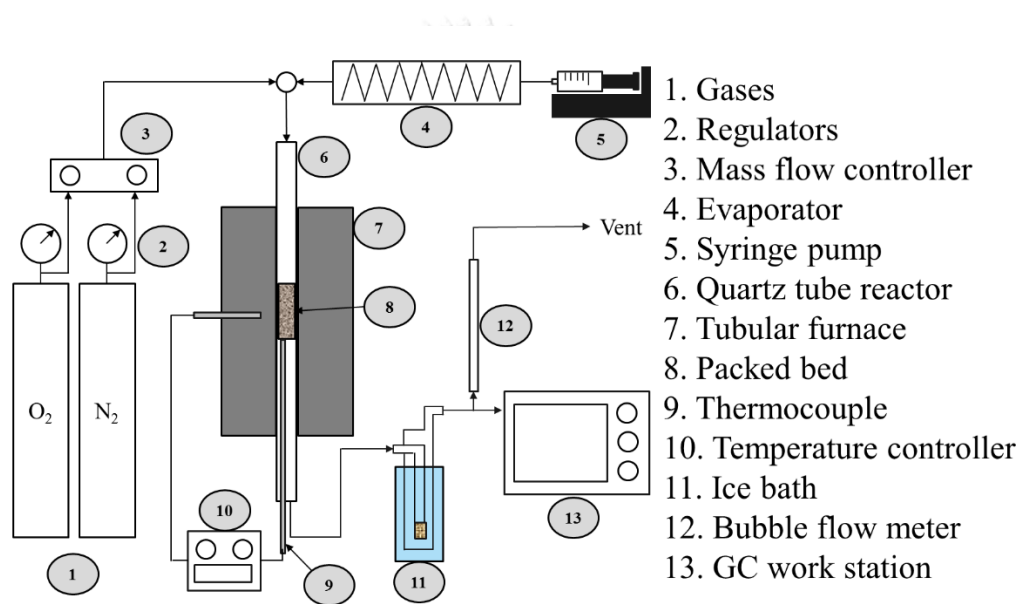
Figure 3.2 Experimental equipment for hydrogen production by chemical looping steam reforming of ethanol

In the fuel feed step, the mixture of water and ethanol with steam to ethanol (S/E) mole ratio of 3 was fed from a liquid phase by a syringe pump (KD Scientific Inc.) with a flow rate of 3.4 ml/h and then it was vaporized and mixed with N_2 carrier gas with a total flow rate of 130 ml/min under a constant WHSV at 6.18 h^{-1}. The outlet stream was trapped by an ice bath and was analyzed using a gas chromatography (Shimadzu GC-8A and Shimadzu GC-14B, Japan). The details and conditions of gas chromatography are presented in Table 3.1.

After the fuel feed step, the air feed step was performed. The gas products were removed by N_2 purge until no residue gas was measured. The air feed step was performed by flowing air at a constant flow rate of 100 ml/min to eliminate coke deposition and oxidize Ni metal into NiO. The exit gas in the air feed step was collected and the amount of CO_2 was analyzed using gas chromatography to obtain the amount of carbon oxidization. The air feed step was stopped when the concentration of oxygen returned to 20 vol.%, indicating that no oxidization reaction further occurred.

All oxygen carriers were studied to investigate long-term redox stability after 5 cycles of operation at $500^{o}C$ at atmospheric pressure.

The activity of oxygen carriers was calculated in terms of ethanol conversion ($X_{ethanol}$) and hydrogen yield (Y_{H2}) as follows:

$$X_{ethanol} = \frac{\dot{n}_{ethanol,in} - \dot{n}_{ethanol,out}}{\dot{n}_{ethanol,in}} \qquad \text{(eq. 1)}$$

$$Y_{H_2} = \frac{\dot{n}_{H_2,out}}{\dot{n}_{ethanol,in}} \qquad \text{(eq. 2)}$$

Table 3.1 Operating conditions for gas chromatography

Gas chromatography	Shimadzu GC-8A		Shimadzu GC-14B
Detector	TCD	TCD	FID
Column	Molecular sieve 5A	Porapak Q	InertCap Wax
- Column material	SUS	SUS	PEG
- Length (m)	2	2	60
- Outer diameter (mm)	4	4	-
- Inner diameter (mm)	3	3	0.32
- Mesh range	60/80	60/80	-
- Maximum temperature (°C)	350	250	250
Carrier gas	Ar (99.999%)	Ar (99.999%)	He (99.999%)
Carrier gas flow (ml/min)	30	30	
Column temperature			
- Initial (°C)	70	70	80
- Final (°C)	70	70	80
Injector temperature (°C)	150	150	150
Detector temperature (°C)	150	150	180
Current (mA)	70	70	-
Analyzed gas	H_2, O_2, N_2, CH_4, CO	CO_2	C_2H_4O, C_2H_6O

CHAPTER IV

RESULTS AND DISCUSSION

4.1 Characterization of fresh oxygen carriers

4.1.1 N_2 adsorption-desorption

Table 4.1 shows physical properties of oxygen carriers (NiO/Al_2O_3) with different addition of rare earth oxide (CeO_2 and La_2O_3) as a promoter. Addition of CeO_2 and La_2O_3 was found to improve the physical properties of NiO/Al_2O_3, especially on decreasing NiO crystallite size (from 20.73 nm to the range of 6-16 nm), resulting in higher surface area, pore volume and pore size, similar to the work of Monica et al. which reported that the modified support by La_2O_3 and CeO_2 leads to an enhancement of the Ni surface area and dispersion [43]. Crystallite size of CeO_2 decreased following to decreasing amount of CeO_2 doped on the support [65]. Among the La_2O_3-CeO_2 promoting oxygen carrier, $NiO/7La_2O_3$-CeO_2-Al_2O_3 exhibited the largest surface area (11.07 m^2/g) and the highest pore volume (0.059 cm^3/g).

Table 4.1 Physical properties of oxygen carriers

Oxygen carrier	Surface area[a] (m^2/g)	Pore volume[a] (cm^3/g)	Pore size[a] (nm)	NiO crystallite size[b] (nm)	CeO$_2$ crystallite size[b] (nm)
NiO/Al$_2$O$_3$	1.36	0.007	14.60	20.73	-
NiO/CeO$_2$-Al$_2$O$_3$	6.58	0.034	29.97	15.99	10.87
NiO/1La$_2$O$_3$-CeO$_2$-Al$_2$O$_3$	6.47	0.023	18.13	13.54	10.33
NiO/3La$_2$O$_3$-CeO$_2$-Al$_2$O$_3$	8.26	0.035	21.94	10.56	9.80
NiO/5La$_2$O$_3$-CeO$_2$-Al$_2$O$_3$	9.79	0.048	23.37	6.64	8.80
NiO/7La$_2$O$_3$-CeO$_2$-Al$_2$O$_3$	11.07	0.059	22.12	7.59	6.47
NiO/9La$_2$O$_3$-CeO$_2$-Al$_2$O$_3$	8.79	0.040	23.46	7.88	3.65
NiO/La$_2$O$_3$-Al$_2$O$_3$	9.55	0.046	20.34	12.31	-

[a] BET

[b] XRD

4.1.2 X-ray diffraction (XRD)

The XRD patterns of the calcined oxygen carriers are shown in Fig. 4.1, showing peaks corresponding to NiO (JCPDS 73-1523; 2θ = 37.3, 43.3, 62.9, 75.4 and 79.3 [25]) and α-Al$_2$O$_3$ rhombohedral structure (JCPDS 88-0826; 2θ = 25.6, 26.8, 35.2, 37.8, 43.4, 52.5, 57.5, 61.3, 66.5, 68.2 and 76.9 [66]) in all samples. The lower intensity and broader peaks of NiO were observed when the promoters were added, corresponding to the smaller crystallite size of NiO when rare earth oxides were introduced onto the Al$_2$O$_3$, presented in Table 4.1.

Ahmed et al. reported that the peaks located at 28° and 49° are attributed to La$_2$O$_3$ (JCPDS 01-089-4016) and the La$_3$O$_3$ peaks are detected when 30 wt.% La-loading on gamma-Al$_2$O$_3$ supported Ni catalyst [67]. In this study, no diffraction peaks of La$_2$O$_3$ for La-doped samples were observed, likely due to small amount of La loading comparing the main composition. It was reported that the La$_3$O$_3$ peaks are not detected for the sample with well formation of solid solution and well

dispersion on the support surface [68]. The work of Navarro et al. reported that the lanthanum exists in the form of a 2-dimensional over layer on alumina and is not detected by XRD for lanthanum loadings below 8.5 mol La/m^2 [69].

The reflections at 2θ of 28.6, 33.2, 47.6, 56.4 and 69.4, which belong to the cubic phase of CeO_2 (JCPDS 34-0394) [11], were detected in NiO/CeO_2-Al_2O_3 sample. In a series of La_2O_3-CeO_2 samples, it was found that the peaks corresponding to CeO_2 shifted to lower degree because of the formation of La_2O_3-CeO_2 solid solution. La^{3+} (ionic radius 0.11 nm) substituted Ce^{4+} (ionic radius 0.097 nm) in the fluorite structure of CeO_2 insulted in an increasing lattice parameter as well as increasing oxygen vacancies which is generated from the charge compensation mechanism. This led to an enhanced oxygen storage capacity and oxygen mobility of the material [70].
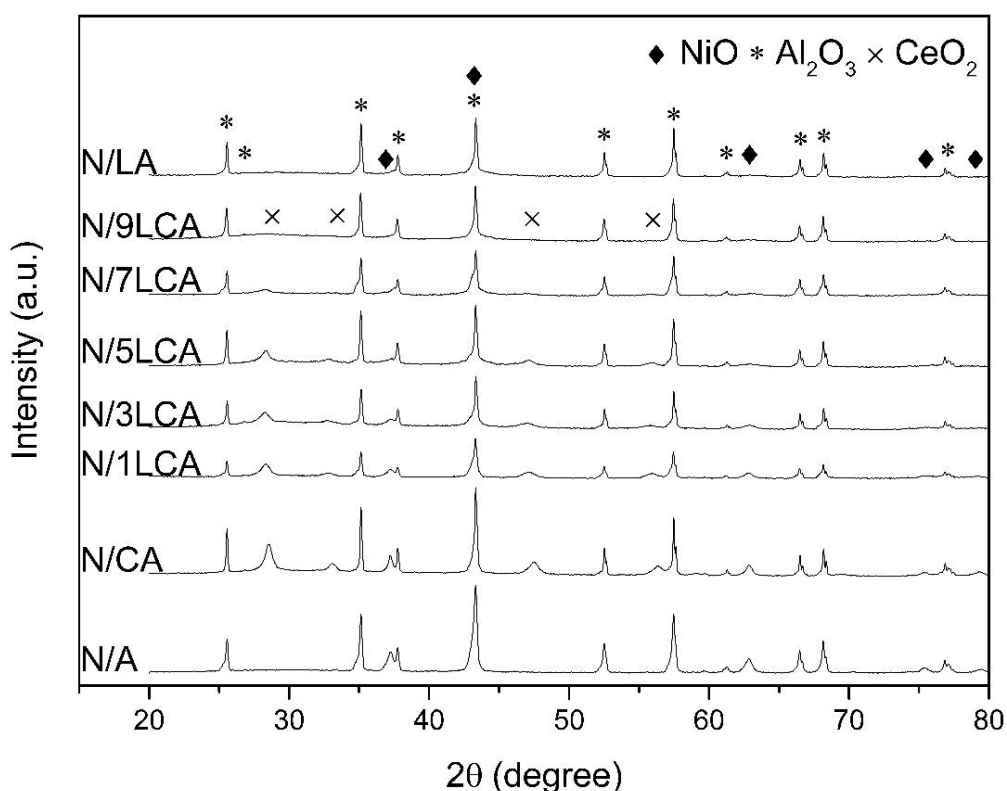

Figure 4.1 XRD patterns of the fresh oxygen carriers

4.1.3 H_2-temperature programmed reduction (H_2-TPR)

The reducibility of oxygen carriers was characterized by H_2-TPR technique. There are 4 main peaks in the temperature range of 150 – 300°C, 300 – 400°C, 400 – 500°C and above 500°C (Fig. 4.2) which represented the reduction of surface-adsorbed oxygen and bulk NiO; NiO species having weak; medium; and, strong interaction with support, respectively [33]. In comparison with NiO/Al_2O_3 oxygen carrier, the area of the third peak of $NiO/CeO_2-Al_2O_3$ decreased while the second peak increased and shifted to lower temperature due to the formation of oxygen vacancies and redox property of Ce (Ce^{4+} to Ce^{3+}) [40].

In case of increasing La-doping on oxygen carrier, area of the first peak increased and the second peak shifted to lower temperature, indicated that more surface-adsorbed oxygen and also Ni species content with weaker metal-support interaction on the surface. The weaker metal-support interaction resulted in easier reduction of NiO and can help accelerating ethanol steam reforming.

Fig. 4.3 displays the temperature at the center of reduction peaks. The first peak of $NiO/CeO_2-Al_2O_3$ (278°C) and $NiO/La_2O_3-Al_2O_3$ (267°C) showed lower temperature than that of NiO/Al_2O_3 (296°C) oxygen carrier. This indicated that Ce-doping and La-doping onto NiO/Al_2O_3 could help improve the reducibility of the oxygen carriers. Furthermore, doping small amount of La_2O_3 could promote thermal stability and enhance the strong metal-support interaction [26, 71] leading to higher temperature of the fourth peak from 452°C (NiO/Al_2O_3) to 564°C ($NiO/La_2O_3-Al_2O_3$).

It should be noted that La-doping oxygen carriers showed an increased reducibility of surface-adsorbed oxygen, bulk NiO and Ni species with weak metal-support interaction, which can further tune by optimizing the ratio of La_2O_3 and CeO_2 [46].
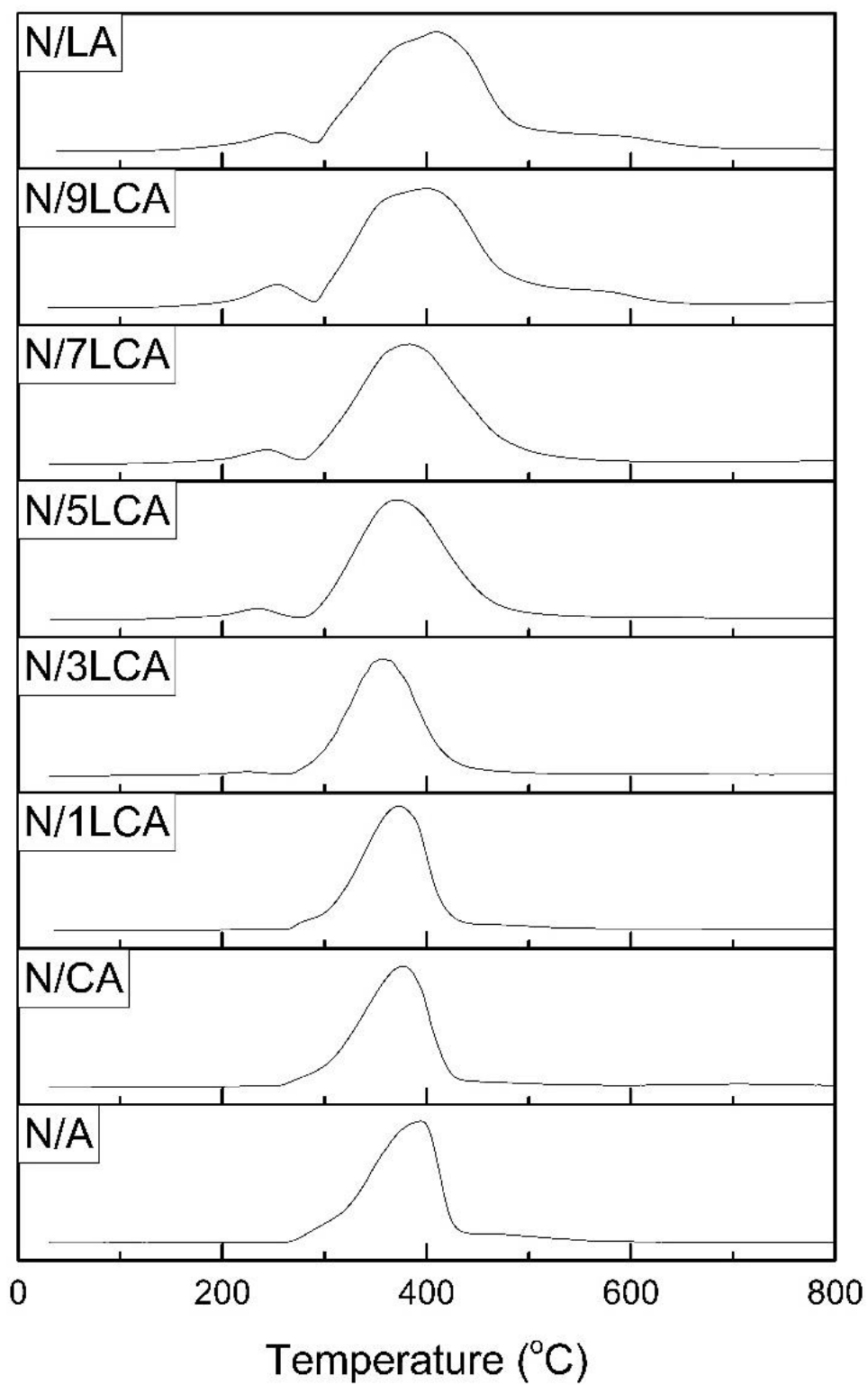
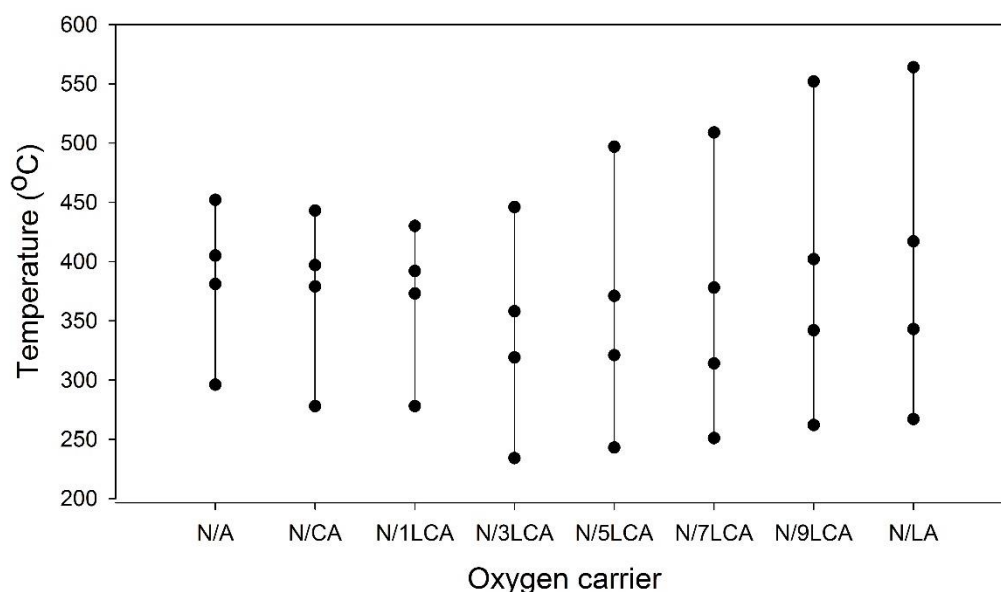**Figure 4.2** H_2-TPR profiles of the oxygen carriers

Figure 4.3 Temperature of center of reduction peak

4.1.4 CO_2-temperature programmed desorption (CO_2-TPD)

CO$_2$-TPD was performed to determine the strength and density of the basicity on oxygen carriers. Generally, types of Lewis basic sites depending on CO_2 desorption temperature comprise weak (<200°C), medium (200 - 400°C), strong (400 - 600°C) and very strong (>600°C) basic sites [67]. From the results in Fig. 4.4, NiO/Al$_2$O$_3$ oxygen carrier exhibited the smallest capacity to adsorb CO_2 on the surface of sample with four desorption peaks centered at 101, 419, 459 and 617°C. Basic property of cerium and lanthanum caused more basic sites on the modified oxygen carriers. Therefore, La-doping significantly improved the strength and density of basicity (Table 4.2) of oxygen carriers in the following sequence: NiO/Al$_2$O$_3$ < NiO/1La$_2$O$_3$-CeO$_2$-Al$_2$O$_3$ < NiO/3La$_2$O$_3$-CeO$_2$-Al$_2$O$_3$ < NiO/CeO$_2$-Al$_2$O$_3$ < NiO/5La$_2$O$_3$-CeO$_2$-Al$_2$O$_3$ < NiO/7La$_2$O$_3$-CeO$_2$-Al$_2$O$_3$ < NiO/9La$_2$O$_3$-CeO$_2$-Al$_2$O$_3$ < NiO/La$_2$O$_3$-Al$_2$O$_3$. In case of NiO/CeO$_2$-Al$_2$O$_3$ oxygen carrier, oxygen storage capacity was improved from the Ce^{3+}/Ce^{4+} redox process. Oxygen vacancy was then increased and the sample could adsorb more amount of CO_2 [72]. La-doping improved basic property and enhanced CO_2 adsorption capacity of the oxygen carrier [73].
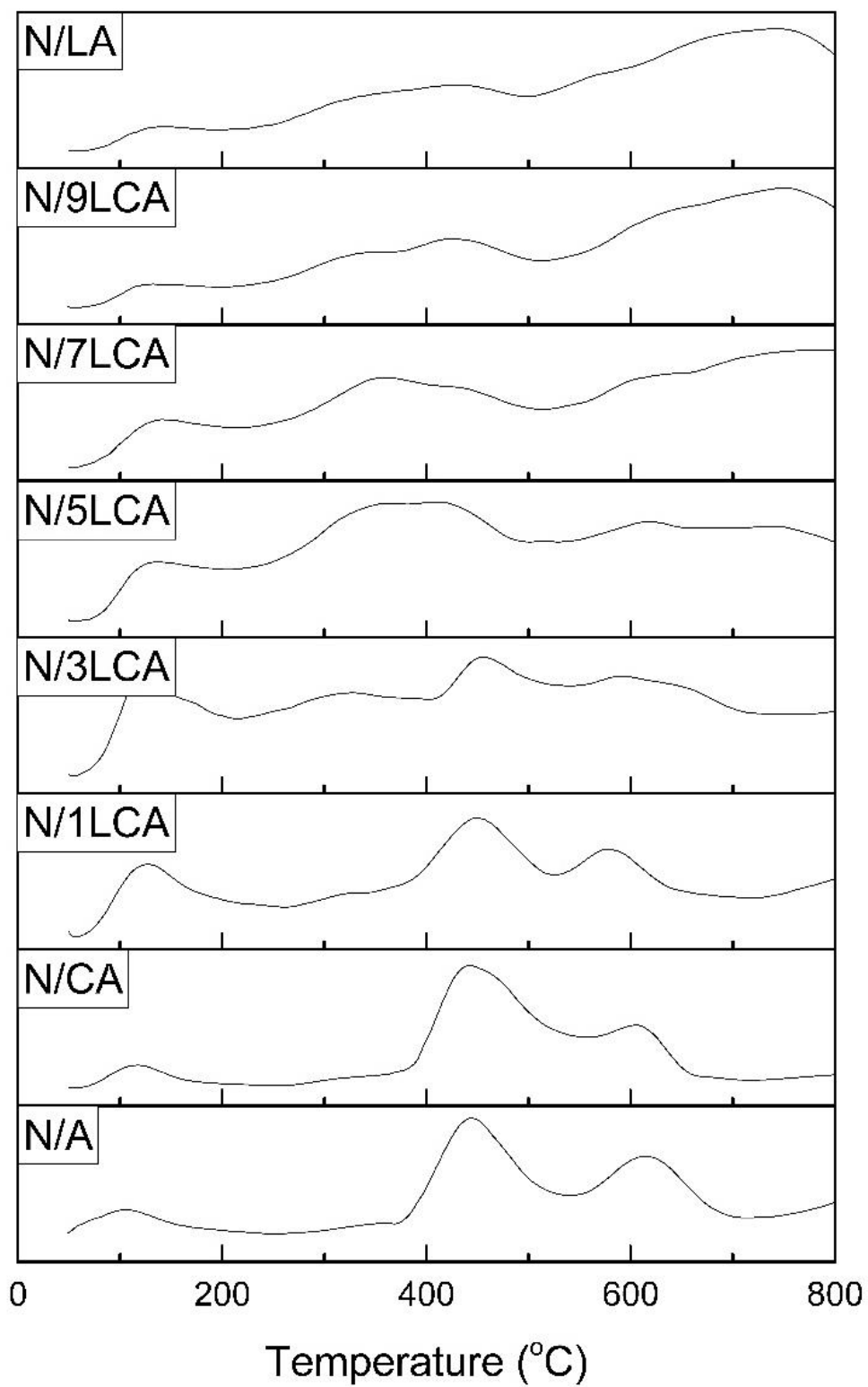
Figure 4.4 CO_2-TPD profiles of the oxygen carriers

Table 4.2 Basicity of oxygen carriers

Oxygen carrier	Basicity (mmol CO_2/g oxygen carrier)
NiO/Al_2O_3	0.3
NiO/CeO_2-Al_2O_3	0.9
NiO/1La_2O_3-CeO_2-Al_2O_3	0.4
NiO/3La_2O_3-CeO_2-Al_2O_3	0.7
NiO/5La_2O_3-CeO_2-Al_2O_3	1.5
NiO/7La_2O_3-CeO_2-Al_2O_3	2.1
NiO/9La_2O_3-CeO_2-Al_2O_3	2.4
NiO/La_2O_3-Al_2O_3	2.6

4.1.5 Scanning electron microscope/Energy dispersive x-ray spectroscopy (SEM/EDX)

The SEM micrographs and EDX mapping of Ni of the fresh oxygen carriers are shown in Fig. 4.5. The morphology of fresh oxygen carriers showed the uniform dispersion of metal on the surface. NiO/CeO_2-Al_2O_3 oxygen carrier showed irregular particle shapes. In case of small amount of La-doping on NiO/CeO_2-Al_2O_3 oxygen carrier, the shapes were similar to those of NiO/CeO_2-Al_2O_3. When amount of La-doping increased the needle-like shapes were observed, presented in Fig. 4.5f – Fig. 4.5h. Ding et al. reported that the strong basicity of La plays an important role in the nucleation and growth of rods. The morphology of La_2O_3 from SEM micrographs are rod-like shapes [74].

From the results, NiO/1La_2O_3-CeO_2-Al_2O_3, NiO/3La_2O_3-CeO_2-Al_2O_3, and NiO/5La_2O_3-CeO_2-Al_2O_3 showed the same morphology as NiO/CeO_2-Al_2O_3 oxygen carriers. On the other hand, NiO/7La_2O_3-CeO_2-Al_2O_3 and NiO/9La_2O_3-CeO_2-Al_2O_3 presented the same morphology as NiO/La_2O_3-Al_2O_3 oxygen carriers. The particle appearance observed by SEM micrographs in this study corresponded well with the solubility limit of La_2O_3-CeO_2 mixed oxides, which is typically between 40 – 70 mol% [75]. However, mixed oxide phases tended to form fluorite crystal structure because

the crystallization temperature of CeO_2 (<450°C) is much lower than La_2O_3 (~700°C) [65].
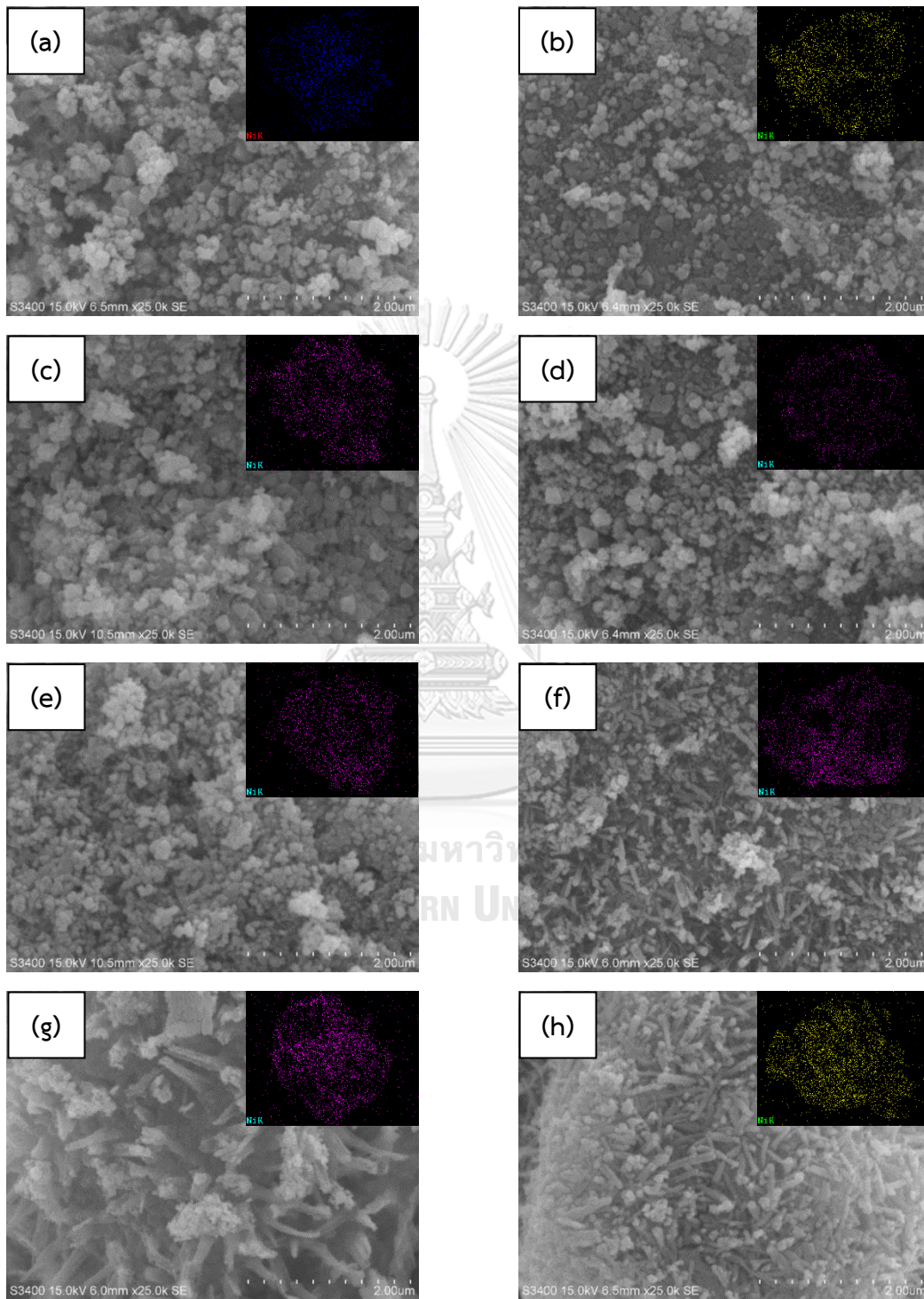
Figure 4.5 SEM micrographs and EDX mapping of Ni of fresh **(a)** N/A **(b)** N/CA **(c)** N/1LCA **(d)** N/3LCA **(e)** N/5LCA **(f)** N/7LCA **(g)** N/9LCA **(h)** N/LA

4.1.6 Thermogravimetry analysis/Differential scanning calorimeter (TGA/DSC)

In chemical looping steam reforming, Ni on the oxygen carrier can be oxidized together with carbon deposition during air feed step. The oxidization rate and oxygen consumption of fresh reduced oxygen carrier were investigated by TGA/DSC in order to compare with the spent oxygen carriers. The reduced oxygen carrier was obtained by 50 vol.% H_2 in N_2 at the temperature of 500°C for 1 hour. The results in Fig. 4.6 showed the DTG profiles of the reduced sample oxidization. Weight loss (increased derivative weight) was observed in the temperature range of room temperature to 200°C, assigned with the dehydration of crystallized water in $La(OH)_3$ structure. Peter et al. studied the reactivity of La_2O_3 powder in air and the results showed that La_2O_3 rapidly hydroxylate to form a stable hydroxide at room temperature [76]. The intensity of the first peak in DTG curve from the dehydration increased with increasing La-doping content. Rare earth oxide improved the oxidization behavior, resulting in the negative peak shifted to lower temperature. The oxidization of Ni/Al_2O_3, $Ni/CeO_2-Al_2O_3$ and $Ni/La_2O_3-Al_2O_3$ oxygen carrier began at the temperature of 285, 255 and 174°C, respectively. It was found that higher area of the first peak in H_2-TPR profiles (Fig. 4.2) displayed lower temperature of the beginning of the oxidization.

The oxidization rate of the sample calculated from the slope of the weight gain with time on stream are shown as black bars in Fig. 4.7. $Ni/7La_2O_3-CeO_2-Al_2O_3$ showed the highest oxidization rate among the $La_2O_3-CeO_2$ doped oxygen carriers. The weight gain during the oxidization step are shown as grey bars in Fig. 4.7. From the H_2-TPR results (Fig. 4.2), 5 wt.% and higher La_2O_3 doped oxygen carriers showed stronger metal-support interaction, which would be reduced at high temperature above 500°C. Therefore, weight gain in $Ni/5La_2O_3-CeO_2-Al_2O_3$, $Ni/7La_2O_3-CeO_2-Al_2O_3$, $Ni/9La_2O_3-CeO_2-Al_2O_3$ and $Ni/La_2O_3-Al_2O_3$ were lower, depending on amount of reduced Ni content on the oxygen carrier.
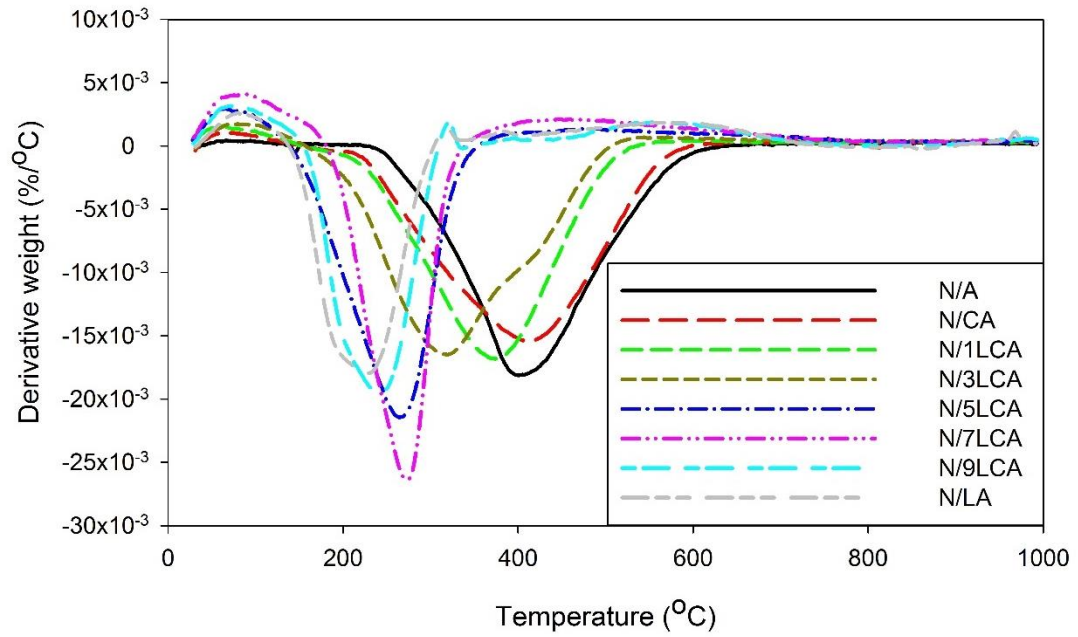
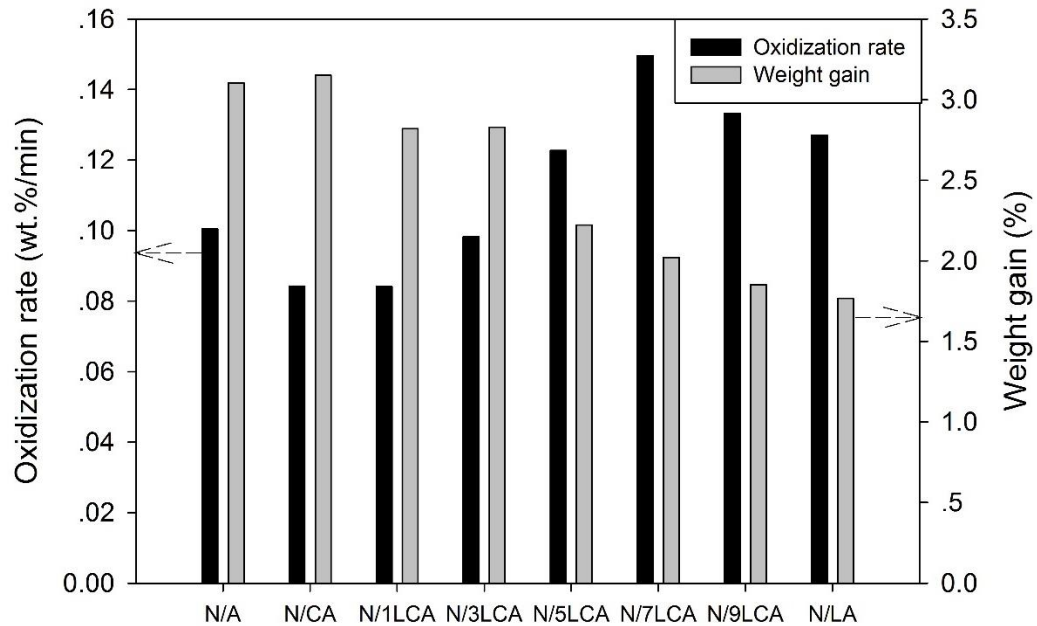**Figure 4.6** DTG profiles of reduced oxygen carriers

Figure 4.7 Oxidization rate and weight gain in oxidization step of reduced oxygen

carriers

4.2 Characterization of reduced oxygen carriers after five cycles of operation

4.2.1 X-ray diffraction (XRD)

The XRD patterns of spent oxygen carriers after the 5th cycle of fuel feed step are presented in Fig. 4.8. All samples exhibited the peak corresponding to cubic Ni crystals (JCPDS 71-1179; 2θ = 44.5, 51.8 and 76.5 [25]) while graphitic carbon deposited on oxygen carriers (2θ = 26.4) was also detected. In addition, the peaks of NiO disappeared for all oxygen carriers, confirming that NiO was converted into metal Ni during the fuel feed step. The characteristic peaks of CeO_2 from spent oxygen carriers located at the same position as those of the fresh oxygen carriers (Fig. 4.1), indicating that the oxygen carriers still remained as a solid solution of La_2O_3-CeO_2 after the 5th cycle of operation.

After five cycles of operation, the peaks of $La_2O_2CO_3$ (2θ = 29.6, 30.4, 33.8, 44.5 and 54.8) and $La(OH)_3$ (2θ = 63.4) were detected from the La-doping oxygen carrier. The surface of La_2O_3 with strong basicity could adsorb CO_2 and formed $La_2O_2CO_3$, reducing carbon deposition on the oxygen carrier thus improving the stability of oxygen carriers [70]. Belliere et al. proved from the XPS results that lanthanum dissolved in cerium with La segregation at its surface at 50 mol% and lower of La in Ce-La solid solution [75]. From this study (Fig. 4.8 (right)), it is observed that La-doped within solubility limits, including NiO/$1La_2O_3$-CeO_2-Al_2O_3, NiO/$3La_2O_3$-CeO_2-Al_2O_3 and NiO/$5La_2O_3$-CeO_2-Al_2O_3, showed low intensity of $La_2O_2CO_3$ at 2θ = 29.6, 30.4 due to the small segregation of La at the surface. In case of NiO/$7La_2O_3$-CeO_2-Al_2O_3, NiO/$9La_2O_3$-CeO_2-Al_2O_3 and NiO/La_2O_3-Al_2O_3, the peak intensity of $La_2O_2CO_3$ increased because larger amount of La_2O_3 particle dispersed on the surface. These results confirmed the solubility limits of La in solid solution structure, prepared by wet impregnation method, was likely at 50 mol%, corresponding to the SEM images in Fig. 4.5. A formation of $La(OH)_3$ was likely due to unstable La_2O_3 phase under ambient as well as hygroscopic nature of La_2O_3 in the moist atmosphere [76, 77].

Table 4.3 shows the crystallite size of reduced Ni after the 5th cycle of fuel feed step. In comparison with the results of fresh oxygen carriers (Table 4.1). It was observed that active Ni was slightly sintered because oxygen carrier was operated under high temperature condition during the reaction.
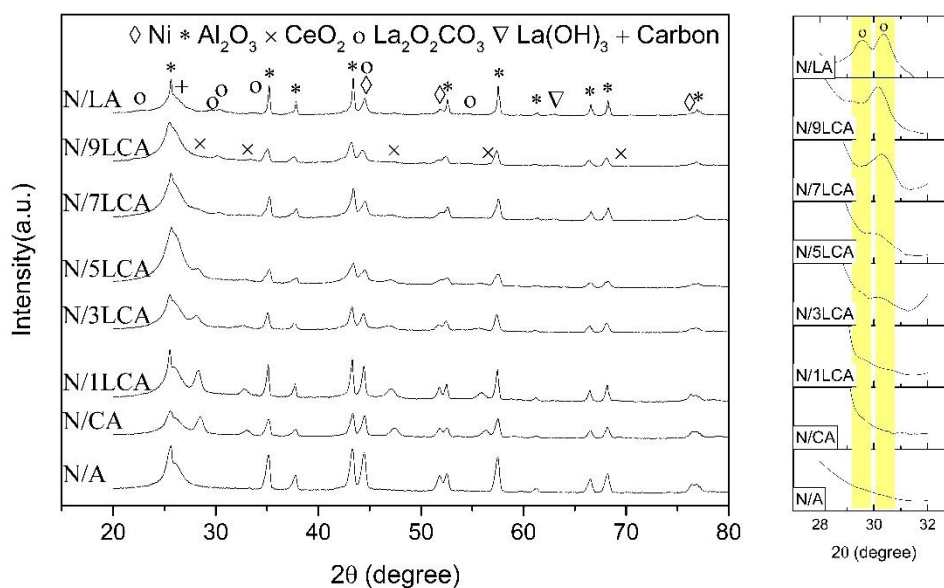
Figure 4.8 XRD patterns of spent oxygen carriers at full scale (left) and details with enlarged scale (right)

Table 4.3 Crystallite size of Ni on reduced oxygen carriers

Oxygen carrier	Ni crystallite size (nm)
NiO/Al_2O_3	22.04
$NiO/CeO_2-Al_2O_3$	16.66
$NiO/1La_2O_3-CeO_2-Al_2O_3$	19.55
$NiO/3La_2O_3-CeO_2-Al_2O_3$	14.68
$NiO/5La_2O_3-CeO_2-Al_2O_3$	11.32
$NiO/7La_2O_3-CeO_2-Al_2O_3$	13.75
$NiO/9La_2O_3-CeO_2-Al_2O_3$	14.48
$NiO/La_2O_3-Al_2O_3$	13.51

4.2.2 Scanning electron microscope/Energy dispersive x-ray spectroscopy (SEM/EDX)

The SEM micrographs of spent oxygen carriers after the 5th cycle of fuel feed step (Fig. 4.9) were obtained to investigate the morphology structure of carbon deposition on the surface. It was observed that fibrous carbon deposited on the surface of all oxygen carriers and led to the decrease in activity of oxygen carriers. Mahadi et al. found that carbon nanofiber is observed on the catalyst from ethanol decomposition reaction, indicating that ethanol is the carbon precursor. The fibrous carbon formation is unavoidable in the CO_2-rich environment [78]. The EDX mapping of Ni on the surface of spent oxygen carriers showed that the active Ni in spent oxygen carriers was less than fresh oxygen carriers (Fig. 4.5) likely due to carbon coverage on active surface, indicating the deactivation of active Ni after operation.
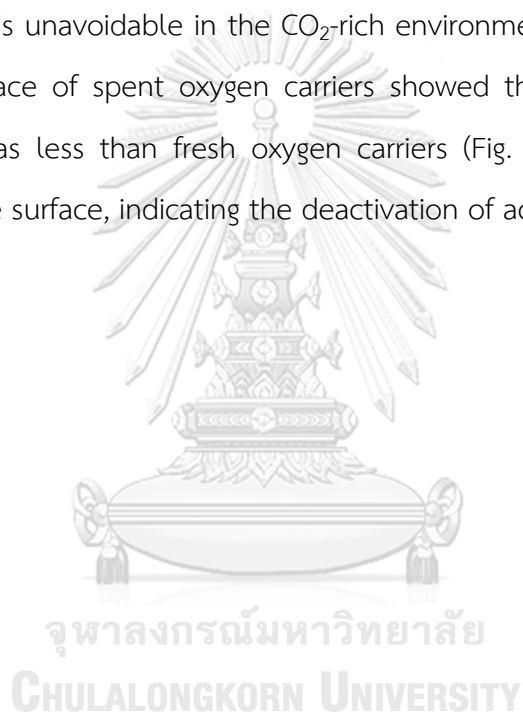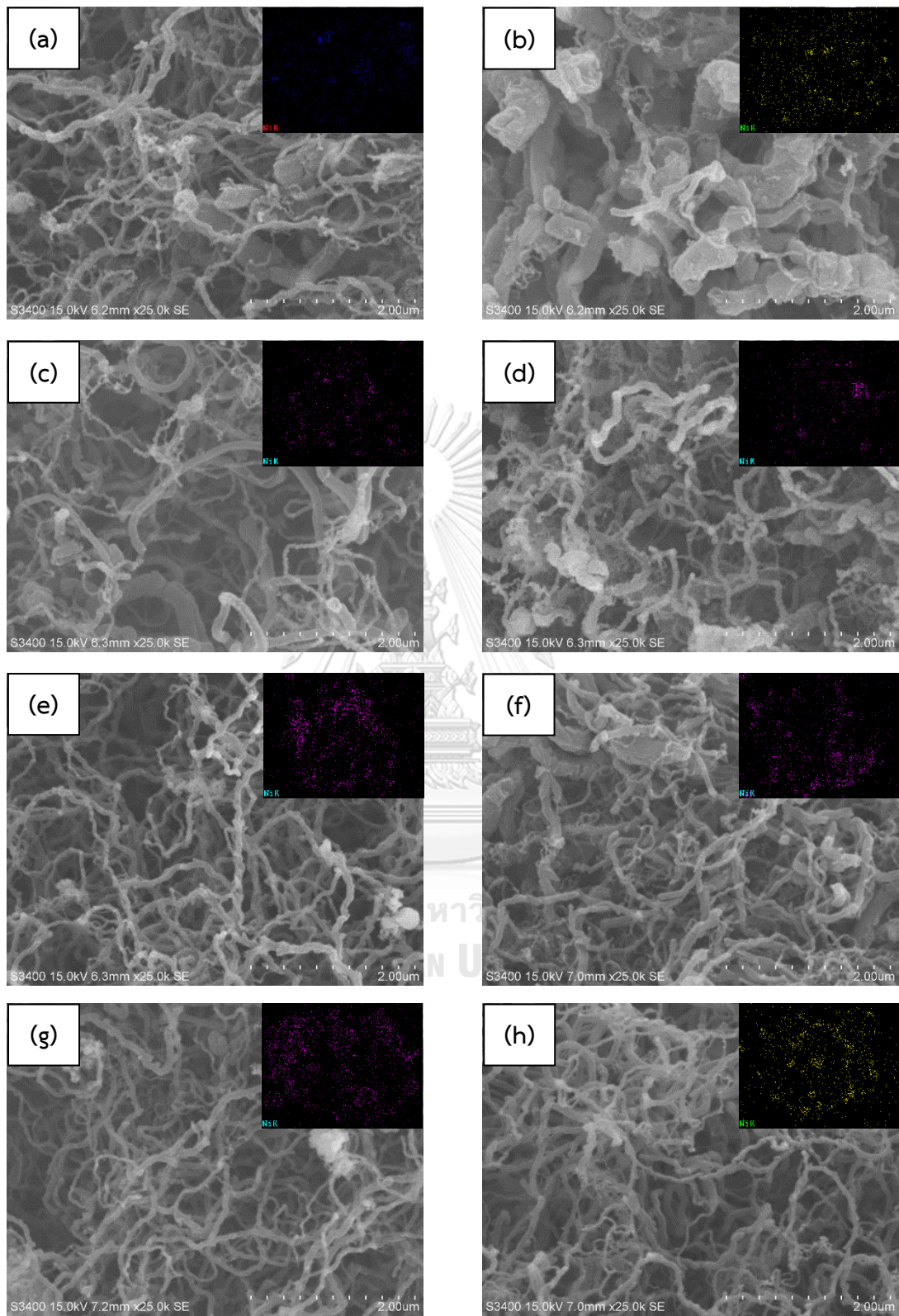
Figure 4.9 SEM micrographs and EDX mapping of Ni of spent **(a)** N/A **(b)** N/CA
(c) N/1LCA **(d)** N/3LCA **(e)** N/5LCA **(f)** N/7LCA **(g)** N/9LCA **(h)** N/LA

4.2.3 Thermogravimetry analysis/Differential scanning calorimeter (TGA/DSC)

After the 5th cycle of fuel feed step, the spent oxygen carriers were heated to 1000°C under air flow condition using TGA to determine the amount of carbon deposition on the oxygen carriers (Fig. 4.10a) and derivative weight (Fig. 4.10b), respectively. Song et al. reported that TPO profiles of spent catalysts can be divided into two regions using 550°C as a borderline, which indicates as amorphous carbon (<550°C) and filamentous carbon (>550°C) [73]. It is well known that filamentous carbon does not severely affect catalyst in steam reforming process while amorphous carbon can encapsulate the active sites until reactant cannot reach to the catalyst sites – significantly affects the catalyst activity [58]. It was reported that carbon deposition are formed from various carbon sources such as (i) intermediate compounds (ethylene, acetaldehyde and acetone), which likely to generate amorphous carbon; (ii) ethanol, which also causes amorphous carbon by means of condensation and dehydrogenation mechanisms; (iii) CO through Boudouard reaction, which causes filamentous carbon; and (iv) CH_4 decomposition, which also causes filamentous carbon [79].

In Fig. 4.10a, carbon deposition was oxidized at temperature above 550°C, indicating filamentous carbon. The spent Ni/La_2O_3-Al_2O_3 showed the largest amount of carbon deposition of 84.17 wt.%, and this value decreased by the following sequence of $Ni/5La_2O_3$-CeO_2-Al_2O_3 (83.95 wt.%) > $Ni/3La_2O_3$-CeO_2-Al_2O_3 (83.12 wt.%) > Ni/CeO_2-Al_2O_3 (79.56 wt.%) > $Ni/1La_2O_3$-CeO_2-Al_2O_3 (78.13 wt.%) > Ni/Al_2O_3 (65.71 wt.%) > $Ni/7La_2O_3$-CeO_2-Al_2O_3 (64.36 wt.%) > $Ni/9La_2O_3$-CeO_2-Al_2O_3 (49.97 wt.%). It can be observed that the peak of derivative weight curves (Fig. 4.10b) of rare-earth doped oxygen carriers shifted to the lower temperature, which indicated that the carbon deposition on the oxygen carriers was easier to be removed [25], likely due to the improved oxygen storage capacity and oxygen mobility.
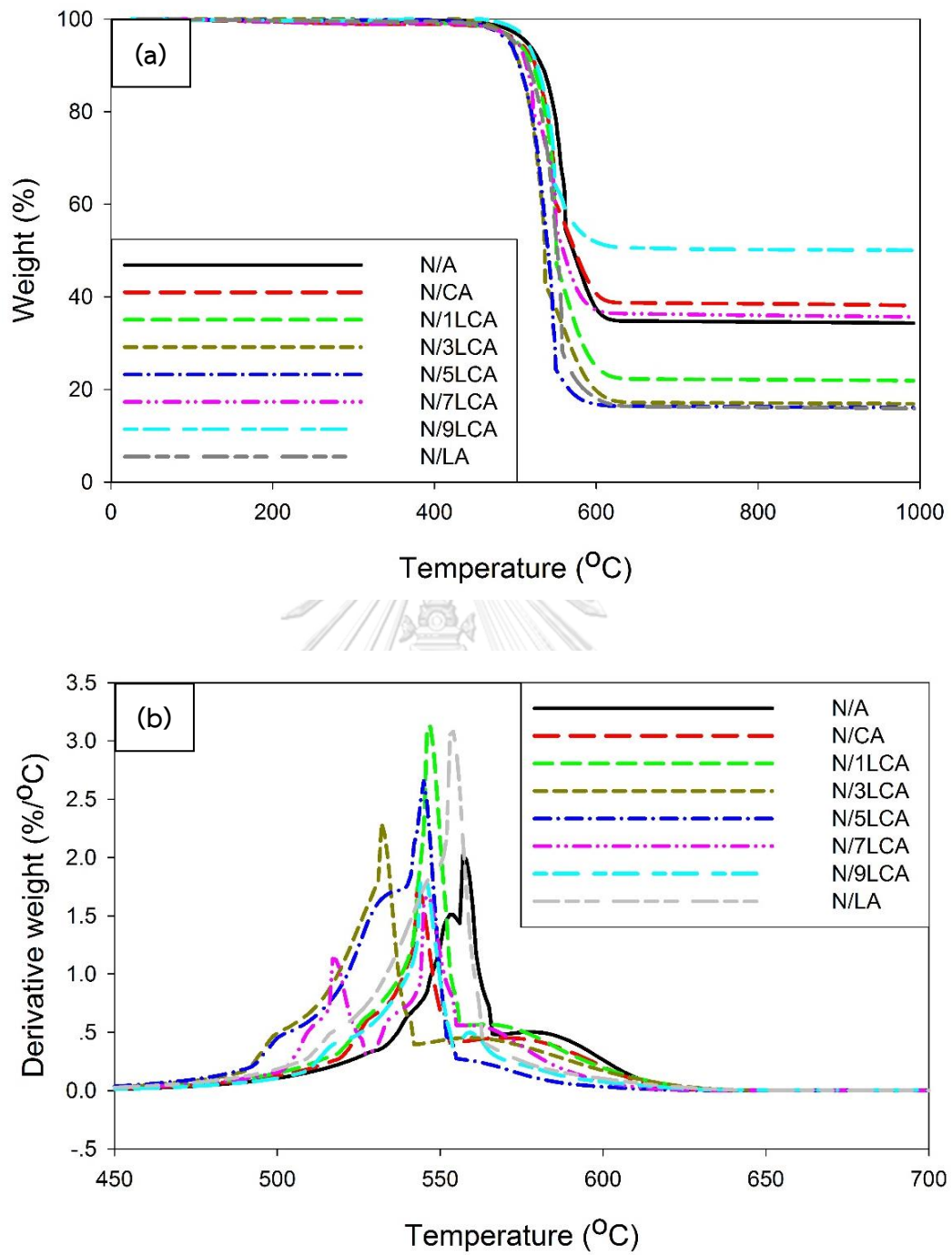
Figure 4.10 (a) TGA and **(b)** DTG profiles of spent oxygen carriers

4.3 Activities of oxygen carriers on chemical looping steam reforming

The activity test of oxygen carriers was evaluated by the conversion of ethanol and H_2 yield from the 1st cycle of chemical looping steam reforming. All of oxygen carriers presented the same trends of conversion of ethanol (Fig. 4.11) – Ethanol conversion increased within 60 minutes and then decreased. The ethanol conversion and H_2 yield (Fig. 4.12) initially increased since NiO was reduced by ethanol to formed metallic Ni which also acts as a catalyst for ethanol steam reforming. After that both conversion and yield decreased, likely due to the deactivation of metallic Ni through carbon deposition. From Fig. 4.11, conversion from NiO/Al_2O_3 oxygen carriers showed the lowest value of time-on-stream at 180 minutes because of severe deactivation from amorphous carbon encapsulating on the catalyst active sites. In case of Ce- and La-doping oxygen carriers, physical properties and basicity property were improved (as mentioned in 4.1.1 and 4.1.4). The basic sites could adsorb CO_2 and reduced carbon deposition on the oxygen carriers. Moreover, Ce-La solid solution in the oxygen carrier structure enhanced oxygen storage capacity and oxygen mobility, then oxygen lattice could diffuse through the structure and could oxidize carbon deposition during the fuel feed step. At 180 minutes time-on-stream, the conversion of ethanol was obtained in the following sequence: $NiO/La_2O_3-Al_2O_3$ (97.83%) > $NiO/5La_2O_3-CeO_2-Al_2O_3$ (96.24%) > $NiO/CeO_2-Al_2O_3$ (95.28%) > $NiO/9La_2O_3-CeO_2-Al_2O_3$ (94.99%) > $NiO/3La_2O_3-CeO_2-Al_2O_3$ (94.95%) > $NiO/7La_2O_3-CeO_2-Al_2O_3$ (86.55%) > $NiO/1La_2O_3-CeO_2-Al_2O_3$ (85.67%) > NiO/Al_2O_3 (83.26%).
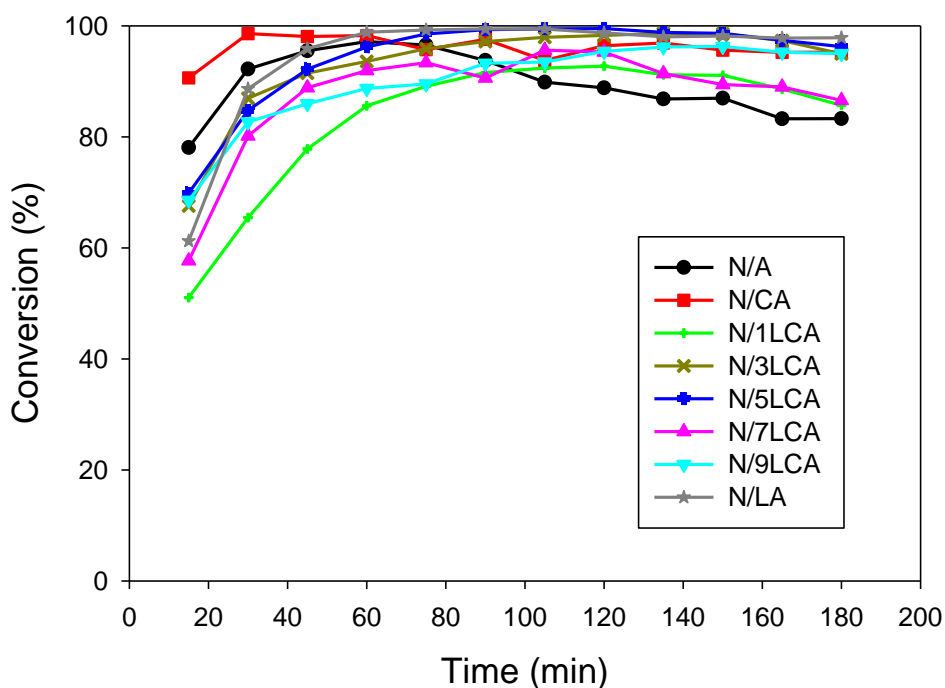
Figure 4.11 Conversion of ethanol at the 1st cycle

During the initial fuel feed step, the period that there was no H_2 generation was called 'dead time'. Unless NiO was sufficiently reduced to Ni, steam reforming of ethanol would not occur. The dead time was considered as a significant indicator for the redox performance of oxygen carriers. Fig. 4.12a shows H_2 yield of the initial 5 minutes of the 1st cycle fuel feed step. The results showed that the highest H_2 yield at 1-minute time-on-stream was obtained by NiO/3La$_2$O$_3$-CeO$_2$-Al$_2$O$_3$ which is the easiest reducible oxygen carrier, according to the lowest temperature of first peak in the H_2-TPR profiles. However, NiO/7La$_2$O$_3$-CeO$_2$-Al$_2$O$_3$ and NiO/La$_2$O$_3$-Al$_2$O$_3$ showed higher H_2 yield at 2-minute time-on-stream than NiO/3La$_2$O$_3$-CeO$_2$-Al$_2$O$_3$ due to higher area of first reducing peak in H_2-TPR profiles. It indicates higher amount of bulk NiO content on the surface which is easily reduce to Ni metal. Moreover, the largest surface area and smaller NiO crystallite size of NiO/7La$_2$O$_3$-CeO$_2$-Al$_2$O$_3$ were the reason for increased H_2 yield.

H$_2$ yield (mol/mol ethanol) at 180 minutes time-on-stream showed in the following sequence of NiO/7La$_2$O$_3$-CeO$_2$-Al$_2$O$_3$ (2.94) > NiO/La$_2$O$_3$-Al$_2$O$_3$ (2.85) > NiO/3La$_2$O$_3$-CeO$_2$-Al$_2$O$_3$ (2.59) > NiO/9La$_2$O$_3$-CeO$_2$-Al$_2$O$_3$ (2.43) > NiO/5La$_2$O$_3$-CeO$_2$-Al$_2$O$_3$ (2.32) > NiO/1La$_2$O$_3$-CeO$_2$-Al$_2$O$_3$ (2.12) > NiO/CeO$_2$-Al$_2$O$_3$ (2.07) > NiO/Al$_2$O$_3$ (1.93).
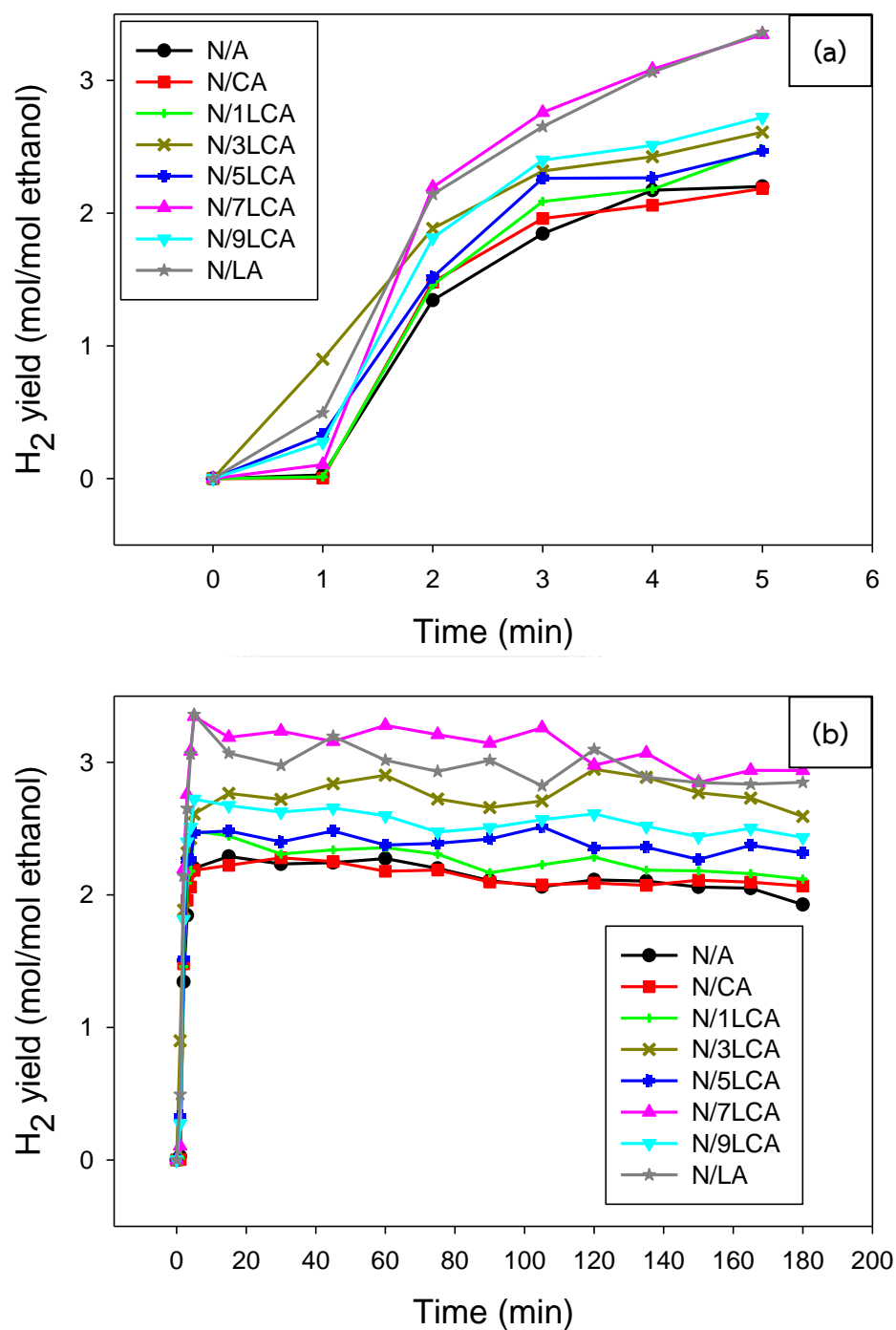

Figure 4.12 H$_2$ yield at 1st cycle

Amount of CO in product stream is shown in Fig. 4.13. NiO/Al_2O_3 showed the highest overall produced CO. In case of modified oxygen carriers, rare earth oxide with strong basic sites improved oxygen storage capacity and oxygen mobility. Therefore, CO generation was inhibited at the beginning of fuel feed step. However, an increased in CO generation later was due to the formation of $La_2O_2CO_3$ and caused a reverse Boudouard reaction, which reduced amorphous carbon deposition on oxygen carriers [67]. Overall amount of CO produced were presented in the following sequence: NiO/Al_2O_3 > $NiO/9La_2O_3$-CeO_2-Al_2O_3 > $NiO/5La_2O_3$-CeO_2-Al_2O_3 > NiO/La_2O_3-Al_2O_3 > $NiO/7La_2O_3$-CeO_2-Al_2O_3 > $NiO/1La_2O_3$-CeO_2-Al_2O_3 > NiO/CeO_2-Al_2O_3 > $NiO/3La_2O_3$-CeO_2-Al_2O_3.
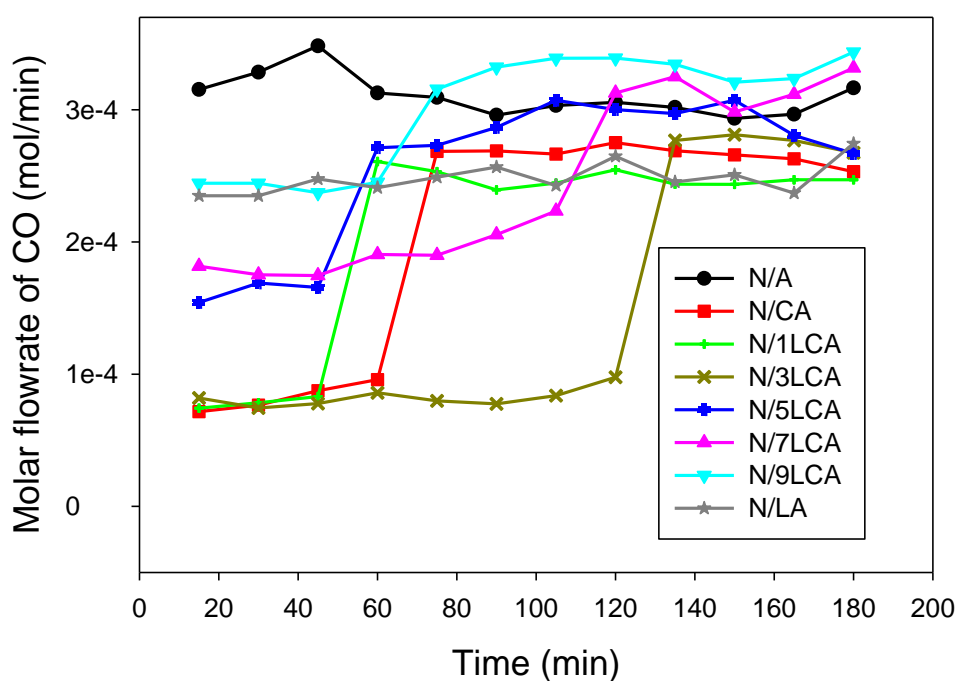

Figure 4.13 Effluent CO flowrate at the 1st cycle

After 3 hours of fuel feed step and no residue gas in the reactor, air (20 vol.% O_2 balanced with N_2) was fed into the reactor to regenerate the oxygen carriers at 500°C. In the air feed step, carbon deposition on the oxygen carriers are oxidized into

CO_2 and active metallic Ni are regenerated to form active NiO. Fig. 4.14 shows the molar flowrate of CO_2 in the exit gas during air feed step. Amount of CO_2 formation can indicate to amount of carbon deposition on oxygen carriers. As mentioned in section 4.2.3, amorphous carbon can be oxidized easier than fibrous carbon (above 550°C). So, it was an amorphous carbon encapsulating on active sites, which was eliminated at the temperature of 500°C during the air feed step. Overall amount of amorphous carbon deposition was presented in the following sequence: NiO/Al_2O_3 > $NiO/1La_2O_3$-CeO_2-Al_2O_3 > NiO/CeO_2-Al_2O_3 > $NiO/3La_2O_3$-CeO_2-Al_2O_3 > $NiO/5La_2O_3$-CeO_2-Al_2O_3 > $NiO/7La_2O_3$-CeO_2-Al_2O_3 > $NiO/9La_2O_3$-CeO_2-Al_2O_3 > NiO/La_2O_3-Al_2O_3. The results showed that as increasing La-doping, carbon deposition decreased. According to CO_2-TPD profiles, La-doping improved basicity property of oxygen carriers and CO_2 adsorption.

Addition of rare earth oxide on NiO/Al_2O_3 helped decreased carbon deposition and also decrease oxygen carrier regeneration duration. This was likely due to an increased oxygen storage capacity by a redox property of Ce^{3+}/Ce^{4+} and an increased oxygen mobility in La_2O_3-CeO_2 solid solution by a lattice distortion of La^{3+} introduced into fluorite structure of CeO_2, which facilitated oxygen lattice diffusion through the structure of oxygen carriers and oxidized carbon deposition on the oxygen carriers during fuel feed step. In case of increasing La-doping over the solubility limit, La^{3+} did not introduce into CeO_2 structure but La_2O_3 dispersed on the surface of oxygen carrier and adsorbed CO_2 using the basic sites to form $La_2O_2CO_3$. Therefore, carbon deposition on the oxygen carrier in this case was removed through the reverse Boudouard reaction on the oxygen carrier's surface. A reduction of carbon deposition could also reduce the heat generation during the air feed step, decreasing the risk of Ni sintering.
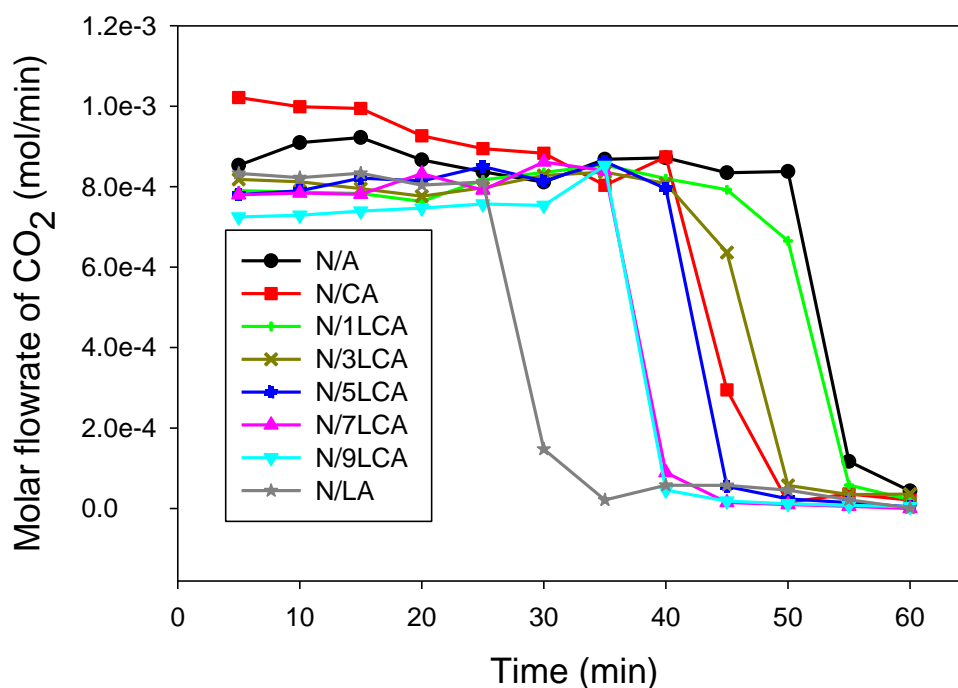
Figure 4.14 Carbon deposition on oxygen carriers at 1st cycle (AFS)

4.4 Stability of oxygen carriers on chemical looping steam reforming

The stability evaluation was conducted at 500°C for 5 cycles of chemical looping steam reforming. Fig. 4.15 presents the conversion of ethanol at the 5th cycle, the deactivation behaviors were observed for all the oxygen carriers. Although NiO/CeO_2-Al_2O_3 oxygen carriers showed the highest conversion during first 2 hours, hydrogen yield (Fig. 4.16) was lower than four other oxygen carriers. $NiO/3La_2O_3$-CeO_2-Al_2O_3 exhibited the highest conversion of ethanol (88.27%) and also H_2 yield (2.46 mol/mol ethanol) at 180-minute time-on-stream. The catalyst also exhibited relatively most stable among other oxygen carriers – ethanol conversion and H_2 yield decreased from the first cycle about 7% and 5%, respectively. Generally, acetaldehyde was formed from ethanol dehydrogenation (reaction (8)) and acetaldehyde decomposed (reaction (12)) to CH_4 and CO. Then, CO reacted with water to produce H_2 through water gas shift reaction (reaction (6)). From Fig. 4.18, acetaldehyde and CO in effluent stream were lower in $NiO/3La_2O_3$-CeO_2-Al_2O_3 than

other oxygen carriers, agreed with the study of Xue et al. reporting that Ce-based supported catalysts favor a pathway of ethanol dehydrogenation to acetaldehyde rather than ethanol dehydration to ethylene and La-doping can give low CO selectivity due to the high water gas shift activity [46]. From the DTG results (Fig. 4.10b), the peak from $NiO/3La_2O_3-CeO2-Al_2O_3$ presented at the lowest temperature, indicating easier carbon deposition removal. From these results, $NiO/3La_2O_3-Al_2O_3$ oxygen carrier showed the lowest deactivation behavior and could be suitable catalyst used for a long-term hydrogen production.
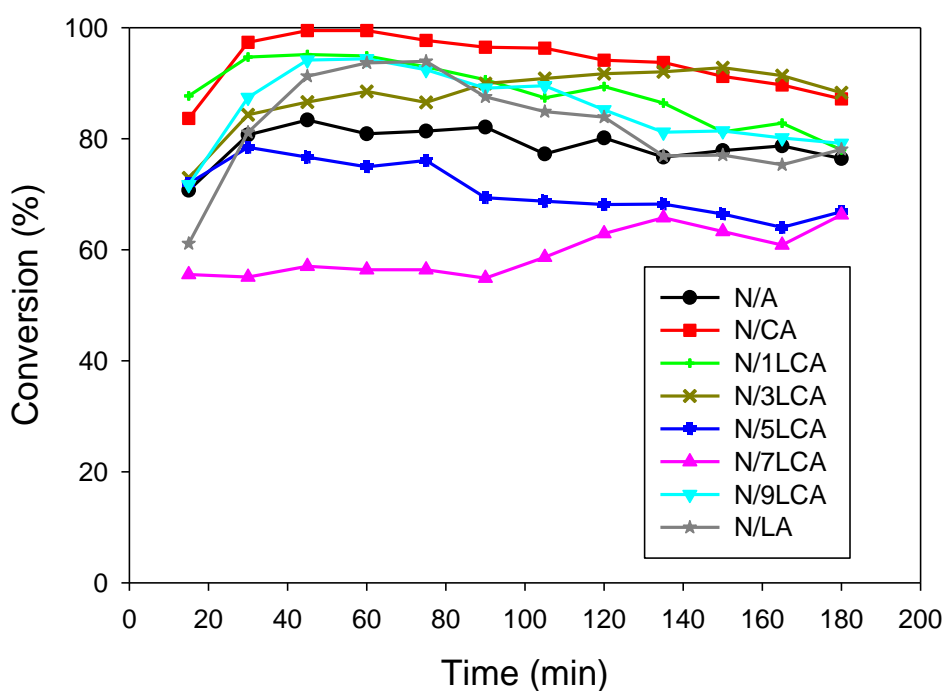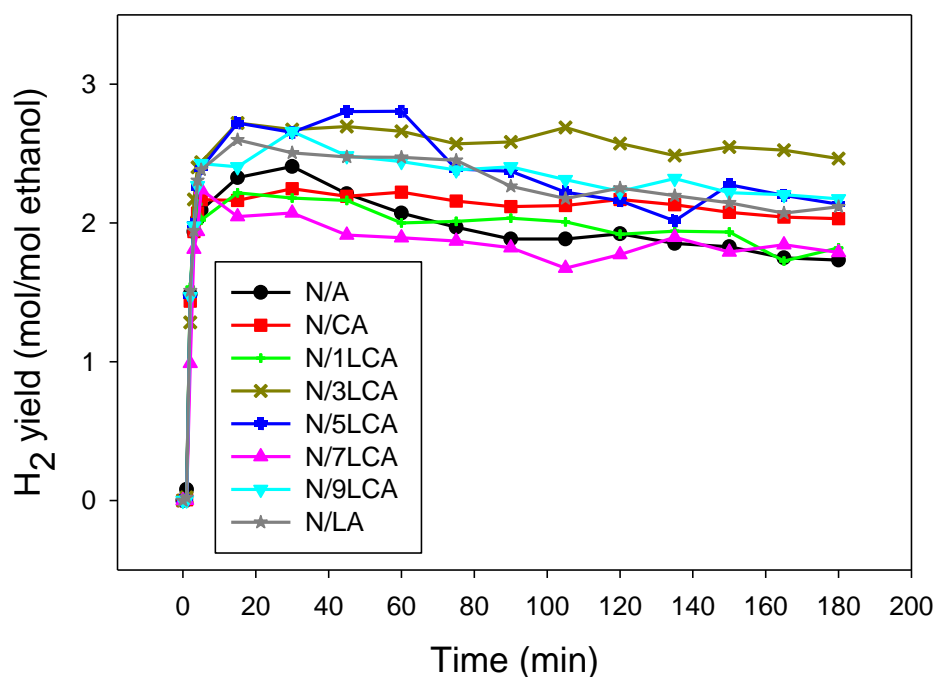

Figure 4.15 Conversion of ethanol at 5th cycle

Figure 4.16 H_2 yield at the 5th cycle

Fig. 4.17 shows the flow rate hydrogen at 5-minute time-on-stream in effluent stream during the fuel feed step of each cycle. In the 1st cycle, NiO/Al_2O_3, NiO/CeO_2-Al_2O_3, $NiO/1La_2O_3$-CeO_2-Al_2O_3 and $NiO/3La_2O_3$-CeO_2-Al_2O_3 presented the same level of hydrogen production. The more La was doped, oxygen carriers showed the higher hydrogen production, likely due to more bulk NiO content dispersed on the surface, confirming by a larger area of the first reduction peak (Fig. 4.2). The bulk NiO was easier to be reduced into Ni metal and acted as catalyst for quick hydrogen production. Moreover, the dispersed La_2O_3 on the surface acted as CO_2 sorbent which facilitated more hydrogen production in the 1st cycle and reduce carbon deposition through the reverse Boudouard reaction. In case of $NiO/5La_2O_3$-CeO_2-Al_2O_3 and higher amount of La_2O_3 on the oxygen carriers, the deactivation behavior was evidently observed at the 2nd to the 5th cycle, which was caused by an irreversible La_2O_3 on the oxygen carriers' surface. According to the XRD patterns of spent oxygen carrier (Fig. 4.8), the peaks of $La_2O_2CO_3$ were observed from the La-doping oxygen

carriers which contained over than 50 mol% of La in solid solution. La_2O_3 could not be regenerated during air feed step at the temperature of 500°C due to $La_2O_2CO_3$ decomposition is endothermic reaction, which can occur at the temperature above 800°C [80]. At elevated temperature where $La_2O_2CO_3$ decomposes into La_2O_3, Ni sintering might occur. Calvin et al. studied the sintering kinetics in the temperature range between 650 to 750°C of Ni-based catalysts in H_2 atmosphere. The results showed that at the temperature above 650°C, the rates of decreasing Ni surface due to Ni sintering are significant, causing 70% loss of the original metal surface area within 50 hours at 750°C [81, 82].
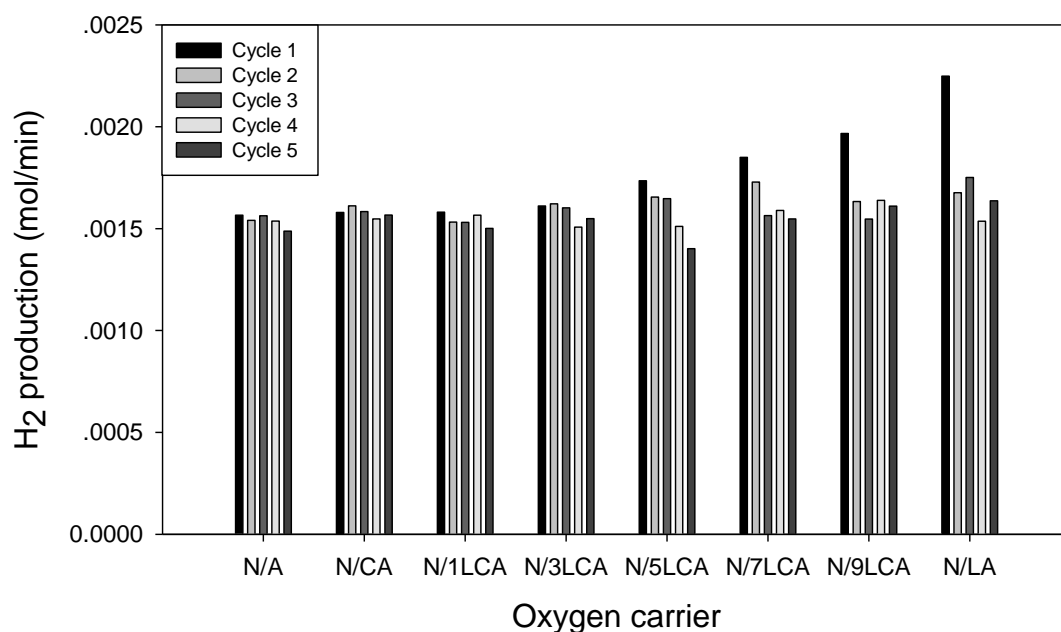

Figure 4.17 Comparison of H_2 yield at 5 minutes time-on-stream

Chemical looping steam reforming of ethanol divided into 2 steps, including fuel feed step and air feed step, which were operated for 180 and 60 minutes, respectively. N_2 purging was introduced for separating each step. Fig 4.18 shows hydrogen production and effluent gases from cycle 1 to cycle 5. Hydrogen production and flowrate of effluent CO_2, CO, and CH_3CHO in fuel feed step was presented for each sample. Carbon deposition was represented by CO_2 molar

flowrate in air feed step. Hydrogen production exhibited the same trend in each cycle – initially increasing and then decreasing. It was observed that when acetaldehyde content in effluent increased and hydrogen content rapidly decreased with more cycle operated. Rare earth oxide-doped on oxygen carriers showed lower amount of CO in effluent stream. Because of larger oxygen storage capacity and oxygen mobility in the structure, CO could be oxidized to CO_2. In case of coke deposition, CO_2 was released about the same level in each cycle of each oxygen carrier.

Figure 4.18 H_2 production (green, square), CO_2 flowrate (purple, triangle down), CO flowrate (red, circle), and CH_3CHO (blue, triangle up) during fuel feed step (left axis) and coke deposition removal (pink, triangle down) during air feed step (right axis) of **(a)** N/A **(b)** N/CA
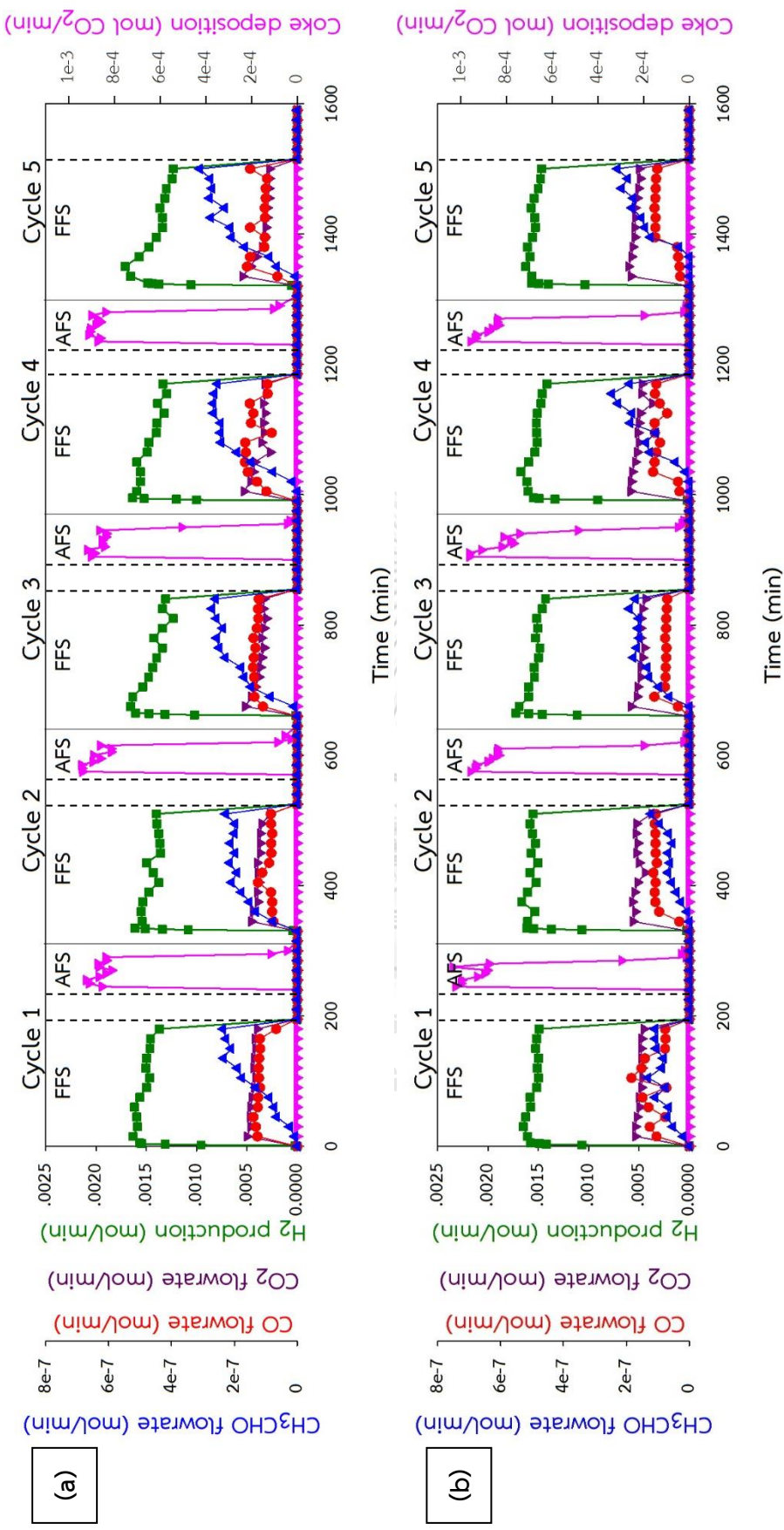
Figure 4.18 (cont.) H_2 production (green, square), CO_2 flowrate (purple, triangle down), CO flowrate (red, circle), and CH_3CHO (blue, triangle down) during air feed step (right axis) of triangle up) during fuel feed step (left axis) and coke deposition removal (pink, triangle down) during air feed step (right axis) of **(c)** N/1LCA **(d)** N/3LCA

Figure 4.18 (cont.) H_2 production (green, square), CO_2 flowrate (purple, triangle down), CO flowrate (red, circle), and CH_3CHO (blue, triangle down) during fuel feed step (left axis) and coke deposition removal (pink, triangle up) during air feed step (right axis) of **(e)** N/5LCA **(f)** N/7LCA
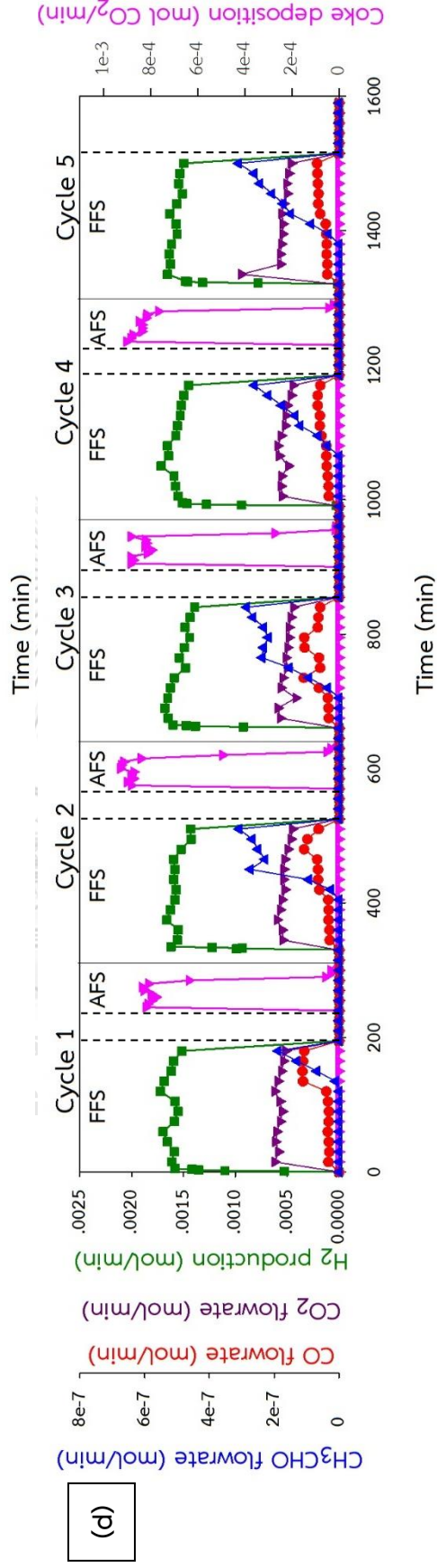
Figure 4.18 (cont.) H_2 production (green, square), CO_2 flowrate (purple, triangle down), CO flowrate (red, circle), and CH_3CHO (blue, triangle down) during air feed step (right axis) of triangle up) during fuel feed step (left axis) and coke deposition removal (pink, triangle down) during air feed step (right axis) of
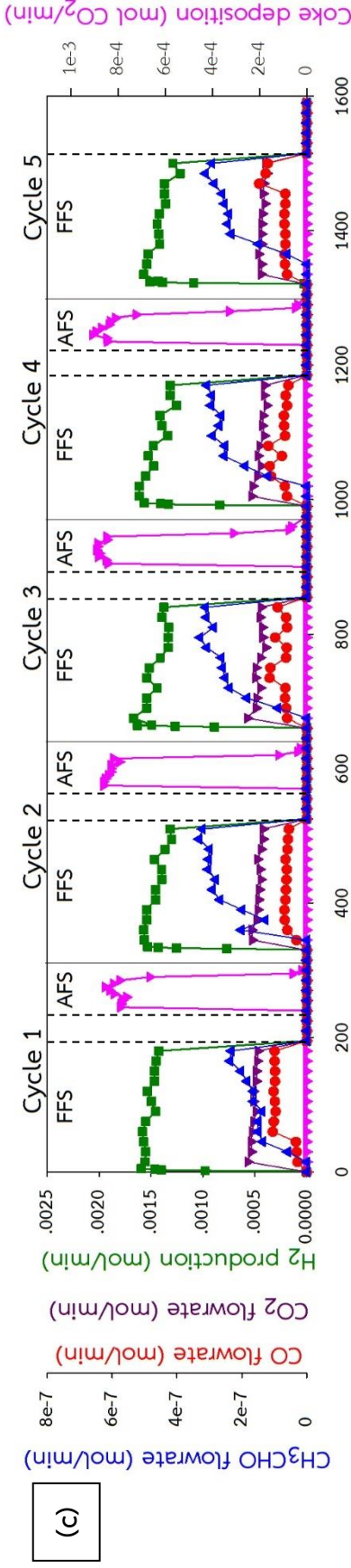
(g) N/9LCA **(h)** N/LA
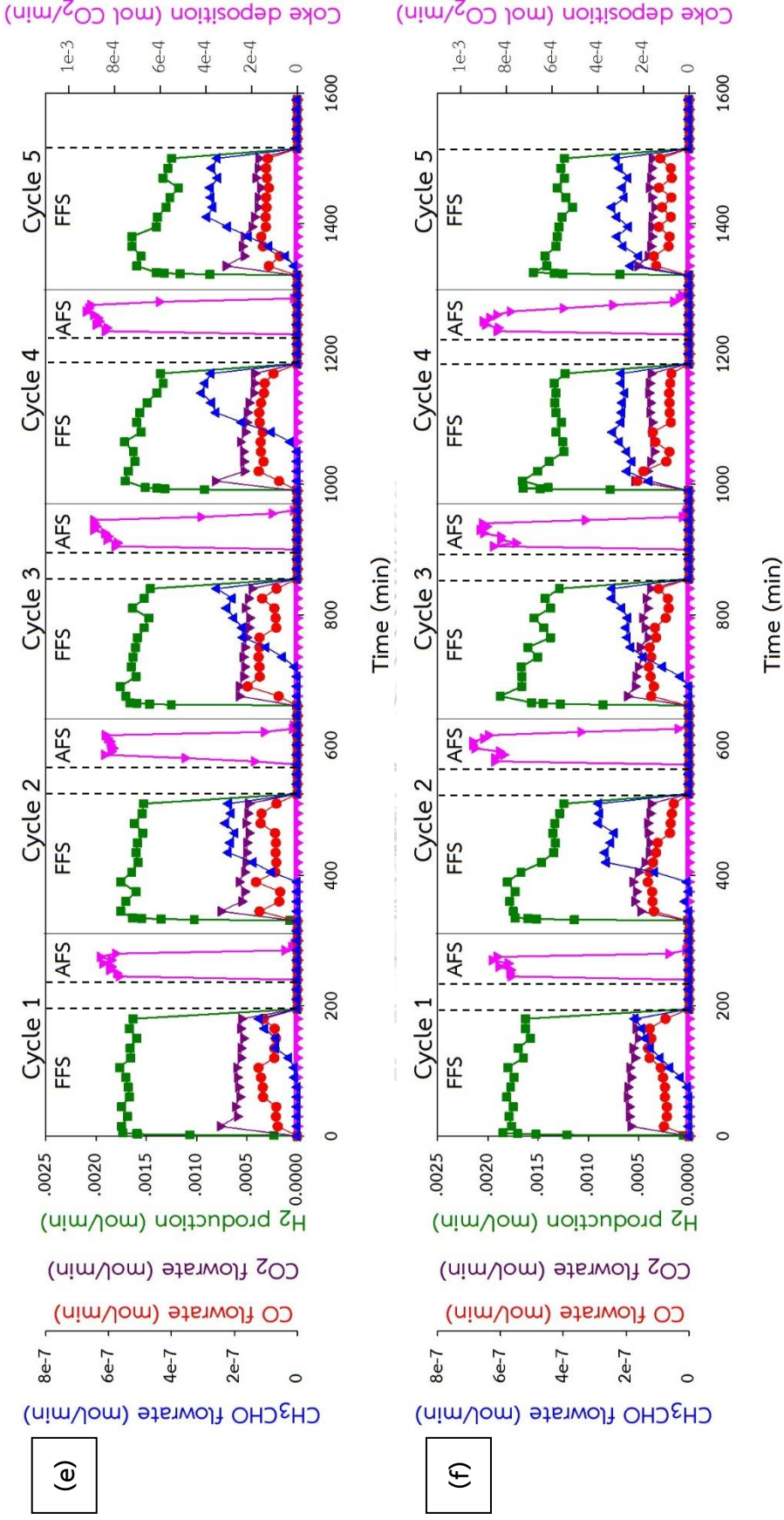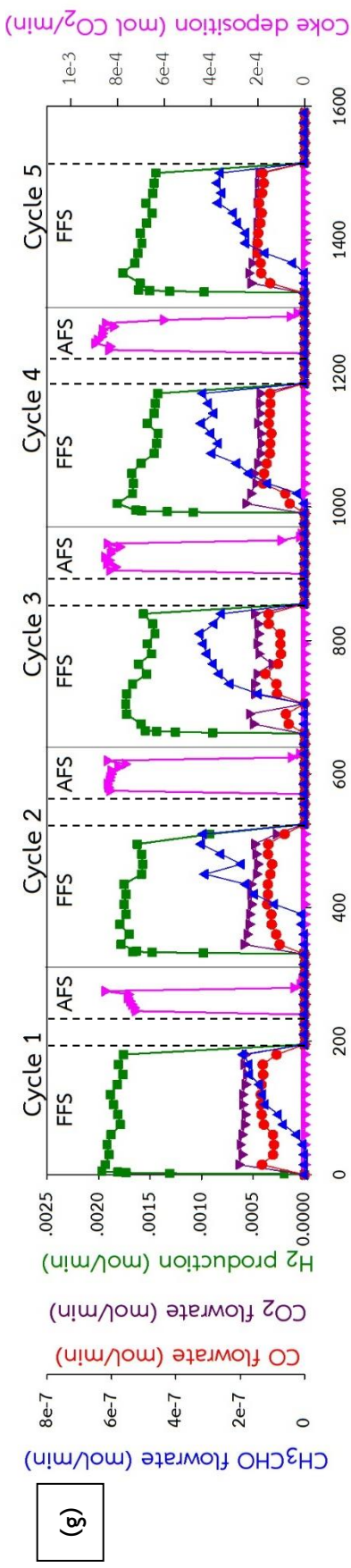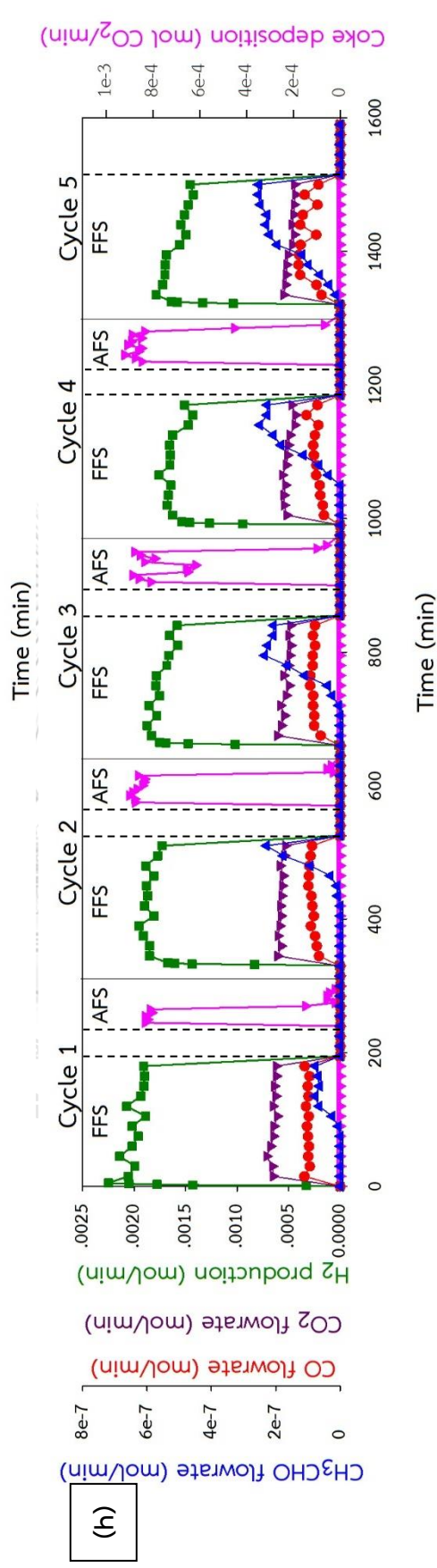
CHAPTER V

CONCLUSION AND RECOMMENDATIONS

5.1 Conclusion

Ni-based oxygen carriers were prepared by wet impregnation method on the alumina support. The addition of Ce^{4+} and La^{3+} into the oxygen carriers decreased Ni crystallite size and increased Ni dispersion, resulting in larger active surface area and easier NiO reduction. As increasing La^{3+}, the surface area initially increased and decreased after reaching its peak at 7 wt.% La_2O_3 (N/7LCA, 12.5wt%Ni/7wt%La_2O_3-3wt%CeO_2-Al_2O_3). The addition of Ce^{4+} and La^{3+} also induced larger Lewis basic sites and more oxygen storage capacity and oxygen mobility. In this study, CeO_2-La_2O_3 solid solution was formed with a solubility limit of La at 50 mol%.

During the first cycle of fuel feed step, all oxygen carriers exhibited rather high ethanol conversion over 80% after 30 minutes time-on-stream, except N/A and N/1LCA which rapidly deactivated. The N/3LCA (12.5wt%Ni/3wt%La_2O_3-7wt%CeO_2-Al_2O_3) was the easiest reducible oxygen carriers according to the H_2-TPR profiles. However, the highest overall hydrogen yield of 3.2 mol H_2/mol ethanol-min was obtained from N/7LCA, which exhibited high surface area (11.07 m_2/g), small NiO crystallite size (7.6 nm), and large basicity site (2.1 mmol CO_2/g oxygen carrier).

Basicity of Ce^{4+} and La^{3+} doped oxygen carriers enhanced the CO_2 adsorption while carbon tolerance of the oxygen carrier was expected to be facilitated through an oxygen storage capacity as well as the formation of $La_2O_2CO_3$. When carbon tolerance increased, regeneration duration of the oxygen carriers during the air feed step decreased. Moreover, decreasing carbon deposition could reduce the heat generation during the air feed step, leading to reduced risk of Ni sintering. Carbon deposition on the modified oxygen carriers also could be removed easier than on the other, verifying by the DTG results.

However, although N/7LCA exhibited the highest H_2 yield at the 1st cycle of operation, after the 5th cycle of operation N/3LCA exhibited the highest conversion of ethanol (88%) and also H_2 yield (2.5 mol/mol ethanol) at 180-minute time-on-stream - decreasing from the first cycle about 7% and 5%, respectively. The ethanol conversion and H_2 yield of N/7LCA significantly decreased from the 1st cycle – 23% and 40%, respectively. Because the regeneration temperature in the air feed step was 500°C which was lower than the decomposition temperature of $La_2O_2CO_3$, the formation of $La_2O_2CO_3$ could not be reversible. Therefore, highly La^{3+} doped oxygen carriers showed relatively lower stability after prolong operation. This suggests that regeneration temperature in air feed step should be elevated when highly La^{3+} doped oxygen carriers was employed, in concerning of Ni sintering at increased temperature.

5.2 Recommendations

From the experimental results, the following recommendations were presented including;

1) The oxygen carrier preparation method should be varied among many methods such as co-precipitation method, sol-gel synthesis method, to improve the physical properties, including higher surface area and small NiO crystallite size.

2) A GC-online unit should be connected in the GC work station to accurately determine the duration of 'dead-time' for each oxygen carrier. Oxygen carrier with the shortest dead-time and high amount of produced H_2 might be more suitable with the fluidized bed system, which can be applied in industry.

3) Another designed reactor, which is using in industry, should be studied, such as, two interconnected fluidized bed reactors, to consider heat balance of the fuel and air reactor in an auto-thermal system.

REFERENCES

[1] Nguyen, V.N., Deja, R., Peters, R., Blum, L., Stolten, D., "Study of the catalytic combustion of lean hydrogen-air mixtures in a monolith reactor", *International Journal of Hydrogen Energy* 43(36) (2018): 17520-17530.

[2] Zhang, C., Hu, X., Zhang, Z., Zhang, L., Dong, D., Gao, G., Westerhof, R., Syed-Hassan, S.S.A., "Steam reforming of acetic acid over Ni/Al_2O_3 catalyst: Correlation of calcination temperature with the interaction of nickel and alumina", *Fuel* 227 (2018): 307-324.

[3] Li, L., Jiang, B., Tang, D., Zhang, Q., Zheng, Z., "Hydrogen generation by acetic acid steam reforming over Ni-based catalysts derived from $La_{1-x}Ce_xNiO_3$ perovskite", *International Journal of Hydrogen Energy* 43(14) (2018): 6795-6803.

[4] Dobosz, J., Małecka, M., Zawadzki, M., "Hydrogen generation via ethanol steam reforming over Co/HAp catalysts", *Journal of the Energy Institute* 91(3) (2018): 411-423.

[5] Aman, D., Radwan, D., Ebaid, M., Mikhail, S., van Steen, E., "Comparing nickel and cobalt perovskites for steam reforming of glycerol", *Molecular Catalysis* 452 (2018): 60-67.

[6] Lei, Y., Luo, Y., Li, X., Lu, J., Mei, Z., Peng, W., Chen, R., Chen, K., Chen, D., He, D., "The role of samarium on Cu/Al_2O_3 catalyst in the methanol steam reforming for hydrogen production", *Catalysis Today* 307 (2018): 162-168.

[7] Parlett, C.M.A., Aydin, A., Durndell, L.J., Frattini, L., Isaacs, M.A., Lee, A.F., Liu, X., Olivi, L., Trofimovaite, R., Wilson, K., Wu, C., "Tailored mesoporous silica supports for Ni catalysed hydrogen production from ethanol steam reforming", *Catalysis Communications* 91 (2017): 76-79.

[8] Park, S., Yoo, J., Han, S.J., Song, J.H., Lee, E.J., Song, I.K., "Steam reforming of liquefied natural gas (LNG) for hydrogen production over nickel–boron–alumina xerogel catalyst", *International Journal of Hydrogen Energy* 42(22) (2017): 15096-15106.

[9] Bepari, S., Basu, S., Pradhan, N.C., Dalai, A.K., "Steam reforming of ethanol over cerium-promoted Ni-Mg-Al hydrotalcite catalysts", *Catalysis Today* 291 (2017): 47-57.

[10] Bepari, S., Pradhan, N.C., Dalai, A.K., "Selective production of hydrogen by steam reforming of glycerol over Ni/Fly ash catalyst", *Catalysis Today* 291 (2017): 36-46.

[11] Kamonsuangkasem, K., Therdthianwong, S., Therdthianwong, A., Thammajak, N., "Remarkable activity and stability of Ni catalyst supported on CeO_2-Al_2O_3 via $CeAlO_3$ perovskite towards glycerol steam reforming for hydrogen production", *Applied Catalysis B: Environmental* 218 (2017): 650-663.

[12] Zamzuri, N.H., Mat, R., Saidina Amin, N.A., Talebian-Kiakalaieh, A., "Hydrogen production from catalytic steam reforming of glycerol over various supported nickel catalysts", *International Journal of Hydrogen Energy* 42(14) (2017): 9087-9098.

[13] He, S., Mei, Z., Liu, N., Zhang, L., Lu, J., Li, X., Wang, J., He, D., Luo, Y., "Ni/SBA-15 catalysts for hydrogen production by ethanol steam reforming: Effect of nickel precursor", *International Journal of Hydrogen Energy* 42(21) (2017): 14429-14438.

[14] Santander, J.A., Tonetto, G.M., Pedernera, M.N., López, E., "Ni/CeO_2–MgO catalysts supported on stainless steel plates for ethanol steam reforming", *International Journal of Hydrogen Energy* 42(15) (2017): 9482-9492.

[15] González-Gil, R., Herrera, C., Larrubia, M.Á., Kowalik, P., Pieta, I.S., Alemany, L.J., "Hydrogen production by steam reforming of DME over Ni-based catalysts modified with vanadium", *International Journal of Hydrogen Energy* 41(43) (2016): 19781-19788.

[16] Shokrollahi Yancheshmeh, M., Radfarnia, H.R., Iliuta, M.C., "High temperature CO_2 sorbents and their application for hydrogen production by sorption enhanced steam reforming process", *Chemical Engineering Journal* 283 (2016): 420-444.

[17] Xie, H., Yu, Q., Zuo, Z., Han, Z., Yao, X., Qin, Q., "Hydrogen production via sorption-enhanced catalytic steam reforming of bio-oil", *International Journal of Hydrogen Energy* 41(4) (2016): 2345-2353.

[18] Shen, Y., Zhao, K., He, F., Li, H., "The structure-reactivity relationships of using three-dimensionally ordered macroporous $LaFe_{1-x}Ni_xO_3$ perovskites for chemical-looping steam methane reforming", *Journal of the Energy Institute* (2018).

[19] Ding, H., Xu, Y., Luo, C., Wang, Q., Shen, C., Xu, J., Zhang, L., "A novel composite perovskite-based material for chemical-looping steam methane reforming to hydrogen and syngas", *Energy Conversion and Management* 171 (2018): 12-19.

[20] Meshksar, M., Daneshmand-Jahromi, S., Rahimpour, M.R., "Synthesis and characterization of cerium promoted Ni/SBA-16 oxygen carrier in cyclic chemical

looping steam methane reforming", *Journal of the Taiwan Institute of Chemical Engineers* 76 (2017): 73-82.

[21] Zhao, K., He, F., Huang, Z., Wei, G., Zheng, A., Li, H., Zhao, Z., "Perovskite-type $LaFe_{1-x}Mn_xO_3$ (x=0, 0.3, 0.5, 0.7, 1.0) oxygen carriers for chemical-looping steam methane reforming: Oxidation activity and resistance to carbon formation", *Korean Journal of Chemical Engineering* 34(6) (2017): 1651-1660.

[22] Wang, W., Fan, L., Wang, G., "Study on chemical looping reforming of ethanol (CLRE) for hydrogen production using $NiMn_2O_4$ spinel as oxygen carrier", *Journal of the Energy Institute* 90(6) (2017): 884-892.

[23] Zhang, Q., Li, L., Jiang, B., Tang, D., Dou, B., "Hydrogen by chemical looping reforming of ethanol: The effect of promoters on $La_{2-x}M_xNi_{4}\lambda$ (M = Ca, Sr and Ce) oxygen carriers", *Chemical Engineering Science* 174 (2017): 259-267.

[24] Li, L., Song, Y., Jiang, B., Wang, K., Zhang, Q., "A novel oxygen carrier for chemical looping reforming: $LaNiO_3$ perovskite supported on montmorillonite", *Energy* 131 (2017): 58-66.

[25] Wang, K., Dou, B., Jiang, B., Zhang, Q., Li, M., Chen, H., Xu, Y., "Effect of support on hydrogen production from chemical looping steam reforming of ethanol over Ni-based oxygen carriers", *International Journal of Hydrogen Energy* 41(39) (2016): 17334-17347.

[26] Wang, K., Dou, B., Jiang, B., Song, Y., Zhang, C., Zhang, Q., Chen, H., Xu, Y., "Renewable hydrogen production from chemical looping steam reforming of ethanol using xCeNi/SBA-15 oxygen carriers in a fixed-bed reactor", *International Journal of Hydrogen Energy* 41(30) (2016): 12899-12909.

[27] Deolalkar, S.P., "Carbon Capture and Storage (CCS)", (2016): 49-58.

[28] Sharma, Y.C., Kumar, A., Prasad, R., Upadhyay, S.N., "Ethanol steam reforming for hydrogen production: Latest and effective catalyst modification strategies to minimize carbonaceous deactivation", *Renewable and Sustainable Energy Reviews* 74 (2017): 89-103.

[29] Contreras, J.L., Salmones, J., Colín-Luna, J.A., Nuño, L., Quintana, B., Córdova, I., Zeifert, B., Tapia, C., Fuentes, G.A., "Catalysts for H_2 production using the ethanol

steam reforming (a review)", *International Journal of Hydrogen Energy* 39(33) (2014): 18835-18853.

[30] Zhang, C., Li, S., Wu, G., Gong, J., "Synthesis of stable Ni-CeO_2 catalysts via ball-milling for ethanol steam reforming", *Catalysis Today* 233 (2014): 53-60.

[31] Sehested, J., "Four challenges for nickel steam-reforming catalysts", *Catalysis Today* 111(1-2) (2006): 103-110.

[32] Cao, A., Lu, R., Veser, G., "Stabilizing metal nanoparticles for heterogeneous catalysis", *Physical Chemistry Chemical Physics* 12(41) (2010): 13499-13510.

[33] Osorio-Vargas, P., Flores-González, N.A., Navarro, R.M., Fierro, J.L.G., Campos, C.H., Reyes, P., "Improved stability of Ni/Al_2O_3 catalysts by effect of promoters (La_2O_3, CeO_2) for ethanol steam-reforming reaction", *Catalysis Today* 259 (2016): 27-38.

[34] Song, J.H., Han, S.J., Yoo, J., Park, S., Kim, D.H., Song, I.K., "Hydrogen production by steam reforming of ethanol over Ni–X/Al_2O_3–ZrO_2 (X = Mg, Ca, Sr, and Ba) xerogel catalysts: Effect of alkaline earth metal addition", *Journal of Molecular Catalysis A: Chemical* 415 (2016): 151-159.

[35] Zafar, Q., Mattisson, T., Gevert, B., "Redox Investigation of Some Oxides of Transition-State Metals Ni, Cu, Fe, and Mn Supported on SiO_2 and $MgAl_2O_4$", *Energy & Fuels* 20 (2006): 34-44.

[36] Karimi, E., Forutan, H.R., Saidi, M., Rahimpour, M.R., Shariati, A., "Experimental Study of Chemical-Looping Reforming in a Fixed-Bed Reactor: Performance Investigation of Different Oxygen Carriers on Al_2O_3 and TiO_2 Support", *Energy & Fuels* 28(4) (2014): 2811-2820.

[37] Trevisanut, C., Vozniuk, O., Mari, M., Urrea, S.Y.A., Lorentz, C., Millet, J.-M.M., Cavani, F., "The Chemical-Loop Reforming of Alcohols on Spinel-Type Mixed Oxides: Comparing Ni, Co, and Fe Ferrite vs Magnetite Performances", *Topics in Catalysis* 59(17-18) (2016): 1600-1613.

[38] Rubel, A., Liu, K., Neathery, J., Taulbee, D., "Oxygen carriers for chemical looping combustion of solid fuels", *Fuel* 88(5) (2009): 876-884.

[39] de Diego, L.F., Ortiz, M., Adánez, J., García-Labiano, F., Abad, A., Gayán, P., "Synthesis gas generation by chemical-looping reforming in a batch fluidized bed

reactor using Ni-based oxygen carriers", *Chemical Engineering Journal* 144(2) (2008): 289-298.

[40] Jiang, B., Li, L., Bian, Z., Li, Z., Othman, M., Sun, Z., Tang, D., Kawi, S., Dou, B., "Hydrogen generation from chemical looping reforming of glycerol by Ce-doped nickel phyllosilicate nanotube oxygen carriers", *Fuel* 222 (2018): 185-192.

[41] Adanez, J., Abad, A., Garcia-Labiano, F., Gayan, P., de Diego, L.F., "Progress in Chemical-Looping Combustion and Reforming technologies", *Progress in Energy and Combustion Science* 38(2) (2012): 215-282.

[42] Li, D., Zeng, L., Li, X., Wang, X., Ma, H., Assabumrungrat, S., Gong, J., "Ceria-promoted Ni/SBA-15 catalysts for ethanol steam reforming with enhanced activity and resistance to deactivation", *Applied Catalysis B: Environmental* 176-177 (2015): 532-541.

[43] Dan, M., Mihet, M., Tasnadi-Asztalos, Z., Imre-Lucaci, A., Katona, G., Lazar, M.D., "Hydrogen production by ethanol steam reforming on nickel catalysts: Effect of support modification by CeO_2 and La_2O_3", *Fuel* 147 (2015): 260-268.

[44] Cheng, Z., Qin, L., Fan, J.A., Fan, L.-S., "New Insight into the Development of Oxygen Carrier Materials for Chemical Looping Systems", *Engineering* 4(3) (2018): 343-351.

[45] Song, H., Ozkan, U., "Ethanol steam reforming over Co-based catalysts: Role of oxygen mobility", *Journal of Catalysis* 261(1) (2009): 66-74.

[46] Han, X., Yu, Y., He, H., Shan, W., "Hydrogen production from oxidative steam reforming of ethanol over rhodium catalysts supported on Ce–La solid solution", *International Journal of Hydrogen Energy* 38(25) (2013): 10293-10304.

[47] Melchor-Hernández, C., Gómez-Cortés, A., Díaz, G., "Hydrogen production by steam reforming of ethanol over nickel supported on La-modified alumina catalysts prepared by sol–gel", *Fuel* 107 (2013): 828-835.

[48] Ni, M., Leung, D.Y.C., Leung, M.K.H., "A review on reforming bio-ethanol for hydrogen production", *International Journal of Hydrogen Energy* 32(15) (2007): 3238-3247.

[49] Lin, K.-H., Wang, C.-B., Chien, S.-H., "Catalytic performance of steam reforming of ethanol at low temperature over LaNiO$_3$ perovskite", *International Journal of Hydrogen Energy* 38(8) (2013): 3226-3232.

[50] Damyanova, S., Pawelec, B., Palcheva, R., Karakirova, Y., Sanchez, M.C.C., Tyuliev, G., Gaigneaux, E., Fierro, J.L.G., "Structure and surface properties of ceria-modified Ni-based catalysts for hydrogen production", *Applied Catalysis B: Environmental* 225 (2018): 340-353.

[51] Bičáková, O., Straka, P., "Production of hydrogen from renewable resources and its effectiveness", *International Journal of Hydrogen Energy* 37(16) (2012): 11563-11578.

[52] Barelli, L., Bidini, G., Gallorini, F., Servili, S., "Hydrogen production through sorption-enhanced steam methane reforming and membrane technology: A review", *Energy* 33(4) (2008): 554-570.

[53] Hafizi, A., Rahimpour, M.R., Hassanajili, S., "Hydrogen production via chemical looping steam methane reforming process: Effect of cerium and calcium promoters on the performance of Fe$_2$O$_3$/Al$_2$O$_3$ oxygen carrier", *Applied Energy* 165 (2016): 685-694.

[54] García-Labiano, F., de Diego, L.F., Adánez, J., Abad, A., Gayán, P., "Temperature variations in the oxygen carrier particles during their reduction and oxidation in a chemical-looping combustion system", *Chemical Engineering Science* 60(3) (2005): 851-862.

[55] Goyal, N., Pant, K.K., Gupta, R., "Hydrogen production by steam reforming of model bio-oil using structured Ni/Al$_2$O$_3$ catalysts", *International Journal of Hydrogen Energy* 38(2) (2013): 921-933.

[56] Li, X., Li, D., Tian, H., Zeng, L., Zhao, Z.-J., Gong, J., "Dry reforming of methane over Ni/La$_2$O$_3$ nanorod catalysts with stabilized Ni nanoparticles", *Applied Catalysis B: Environmental* 202 (2017): 683-694.

[57] Wolfbeisser, A., Sophiphun, O., Bernardi, J., Wittayakun, J., Föttinger, K., Rupprechter, G., "Methane dry reforming over ceria-zirconia supported Ni catalysts", *Catalysis Today* 277 (2016): 234-245.

[58] Montero, C., Ochoa, A., Castaño, P., Bilbao, J., Gayubo, A.G., "Monitoring Ni^0 and coke evolution during the deactivation of a $Ni/La_2O_3–\alpha Al_2O_3$ catalyst in ethanol steam reforming in a fluidized bed", *Journal of Catalysis* 331 (2015): 181-192.

[59] Tsipouriari, V.A., Verykios, X.E., "Kinetic study of the catalytic reforming of methane with carbon dioxide to synthesis gas over Ni/La_2O_3 catalyst", *Catalysis Today* 64 (2001): 83-90.

[60] Tsipouriari, V.A., Verykios, X.E., "Carbon and Oxygen Reaction Pathways of CO_2 Reforming of Methane over Ni/La_2O_3 and Ni/Al_2O_3 Catalysts Studied by Isotopic Tracing Techniques", *Journal of Catalysis* 187 (1999): 85-94.

[61] Mulewa, W., Tahir, M., Amin, N.A.S., "MMT-supported Ni/TiO_2 nanocomposite for low temperature ethanol steam reforming toward hydrogen production", *Chemical Engineering Journal* 326 (2017): 956-969.

[62] Zhao, X., Lu, G., "Modulating and controlling active species dispersion over Ni–Co bimetallic catalysts for enhancement of hydrogen production of ethanol steam reforming", *International Journal of Hydrogen Energy* 41(5) (2016): 3349-3362.

[63] Han, S.J., Bang, Y., Song, J.H., Yoo, J., Park, S., Kang, K.H., Song, I.K., "Hydrogen production by steam reforming of ethanol over dual-templated $Ni–Al_2O_3$ catalyst", *Catalysis Today* 265 (2016): 103-110.

[64] Anjaneyulu, C., Costa, L.O.O.d., Ribeiro, M.C., Rabelo-Neto, R.C., Mattos, L.V., Venugopal, A., Noronha, F.B., "Effect of Zn addition on the performance of Ni/Al_2O_3 catalyst for steam reforming of ethanol", *Applied Catalysis A: General* 519 (2016): 85-98.

[65] Liang, S., Broitman, E., Wang, Y., Cao, A., Veser, G., "Highly stable, mesoporous mixed lanthanum–cerium oxides with tailored structure and reducibility", *Journal of Materials Science* 46(9) (2010): 2928-2937.

[66] Sriharan, N., Ganesan, N.M., Kang, M., Kungumadevi, L., Senthil, T.S., "Improved photoelectrical performance of single crystalline rutile TiO_2 nanorod arrays incorporating α-alumina for high efficiency dye-sensitized solar cells", *Materials Letters* 237 (2019): 204-208.

[67] Al-Fatesh, A.S., Naeem, M.A., Fakeeha, A.H., Abasaeed, A.E., "Role of La_2O_3 as Promoter and Support in Ni/γ-Al_2O_3 Catalysts for Dry Reforming of Methane", *Chinese Journal of Chemical Engineering* 22(1) (2014): 28-37.

[68] Bahari, M.B., Goo, B.C., Pham, T.L.M., Siang, T.J., Danh, H.T., Ainirazali, N., Vo, D.-V.N., "Hydrogen-rich Syngas Production from Ethanol Dry Reforming on La-doped Ni/Al_2O_3 Catalysts: Effect of Promoter Loading", *Procedia Engineering* 148 (2016): 654-661.

[69] Navarro, R.M., Guil-Lopez, R., Ismail, A.A., Al-Sayari, S.A., Fierro, J.L.G., "Ni- and PtNi-catalysts supported on Al_2O_3 for acetone steam reforming: Effect of the modification of support with Ce, La and Mg", *Catalysis Today* 242 (2015): 60-70.

[70] Li, X., Zhao, Z.J., Zeng, L., Zhao, J., Tian, H., Chen, S., Li, K., Sang, S., Gong, J., "On the role of Ce in CO_2 adsorption and activation over lanthanum species", *Chem Sci* 9(14) (2018): 3426-3437.

[71] Li, Y.-f., He, Y.-h., Liu, G.-q., Zeng, L.-w., "Influence of La precursors on structure and properties of CeO_2-ZrO_2-Al_2O_3 composite oxides", *Transactions of Nonferrous Metals Society of China* 28(4) (2018): 739-747.

[72] Abou Rached, J., Cesario, M.R., Estephane, J., Tidahy, H.L., Gennequin, C., Aouad, S., Aboukaïs, A., Abi-Aad, E., "Effects of cerium and lanthanum on Ni-based catalysts for CO_2 reforming of toluene", *Journal of Environmental Chemical Engineering* 6(4) (2018): 4743-4754.

[73] Song, J.H., Yoo, S., Yoo, J., Park, S., Gim, M.Y., Kim, T.H., Song, I.K., "Hydrogen production by steam reforming of ethanol over Ni/Al_2O_3-La_2O_3 xerogel catalysts", *Molecular Catalysis* 434 (2017): 123-133.

[74] Ding, J., Wu, Y., Sun, W., Li, Y., "Preparation of $La(OH)_3$ and La_2O_3 with Rod Morphology by Simple Hydration of La_2O_3", *Journal of Rare Earths* 24(4) (2006): 440-442.

[75] Belliere, V., Joorst, G., Stephan, O., Groot, F.M.F.d., M.Weckhuysen, B., "Phase Segregation in Cerium-Lanthanum Solid Solutions", *Journal of Physical Chemistry B* 110 (2006): 9984-9990.

[76] Fleming, P., Farrell, R.A., Holmes, J.D., Morris, M.A., "The Rapid Formation of La(OH)$_3$ from La$_2$O$_3$ Powders on Exposureto Water Vapor", *Journal of the American Ceramic Society* 93(4) (2010): 1187-1194.

[77] Kang, J.-G., Kim, Y.-I., Won Cho, D., Sohn, Y., "Synthesis and physicochemical properties of La(OH)$_3$ and La$_2$O$_3$ nanostructures", *Materials Science in Semiconductor Processing* 40 (2015): 737-743.

[78] Bahari, M.B., Phuc, N.H.H., Alenazey, F., Vu, K.B., Ainirazali, N., Vo, D.-V.N., "Catalytic performance of La-Ni/Al$_2$O$_3$ catalyst for CO$_2$ reforming of ethanol", *Catalysis Today* 291 (2017): 67-75.

[79] Vicente, J., Ereña, J., Montero, C., Azkoiti, M.J., Bilbao, J., Gayubo, A.G., "Reaction pathway for ethanol steam reforming on a Ni/SiO$_2$ catalyst including coke formation", *International Journal of Hydrogen Energy* 39(33) (2014): 18820-18834.

[80] Svoboda, K., Leitner, J., Havlica, J., Hartman, M., Pohorelý, M., Brynda, J., Šyc, M., Chyou, Y.-P., Chen, P.-C., "Thermodynamic aspects of gasification derived syngas desulfurization, removal of hydrogen halides and regeneration of spent sorbents based on La$_2$O$_3$/La$_2$O$_2$CO$_3$ and cerium oxides", *Fuel* 197 (2017): 277-289.

[81] Bartholomew, C.H., Sorensen, W.L., "Sintering kinetics of silica- and alumina-supported nickel in hydrogen atmosphere", *Journal of Catalysis* 81 (1983): 131-141.

[82] Argyle, M., Bartholomew, C., "Heterogeneous Catalyst Deactivation and Regeneration: A Review", *Catalysts* 5(1) (2015): 145-269.

APPENDIX

APPENDIX A

CALIBRATION CURVES

Calibration curves was done from gas chromatography (Shimadzu GC-8A and Shimadzu GC-14B) with the operating conditions as mentioned in Table 3.1. The gas and liquid standard were injected into gas chromatography at different concentrations. Peak area for each concentration was analyzed from gas chromatography. Then, calibration curves were plotted between peak area and mole of the sample injected into gas chromatography. Fig. A.1 – Fig. A.8 presented the calibration curves for H_2, N_2, O_2, CH_4, CO, CO_2, C_2H_4O, and C_2H_6O, respectively.

$$y = 2.655E\text{-}12x + 5.136E\text{-}08$$
$$R^2 = 9.995E\text{-}01$$
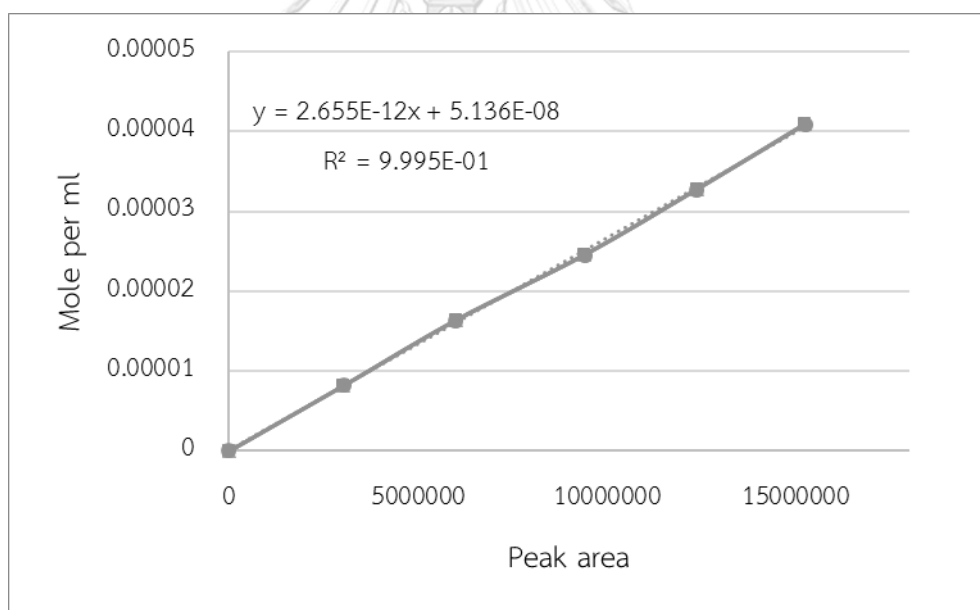
Figure A.1 Calibration curve of H_2
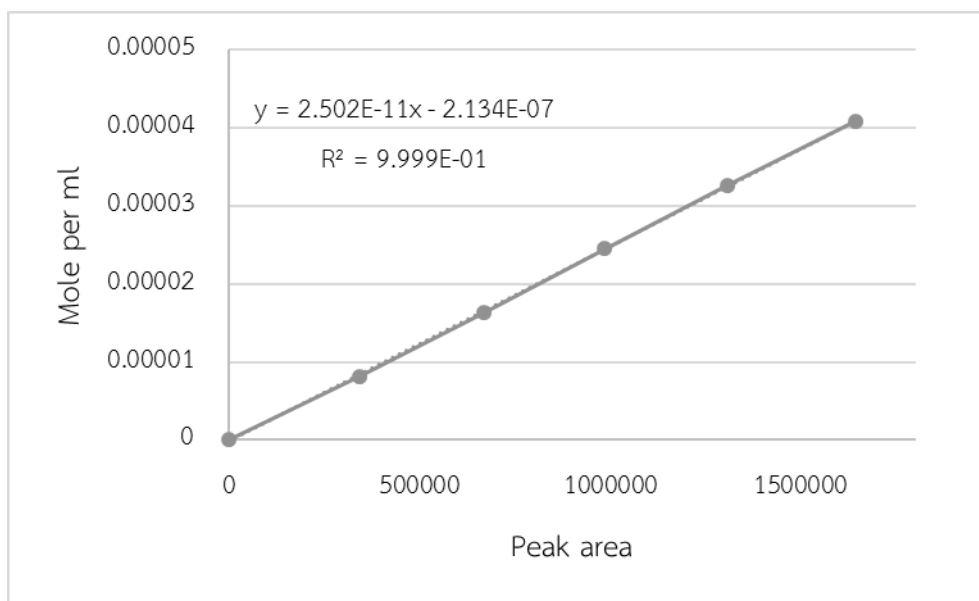
Figure A.2 Calibration curve of N_2
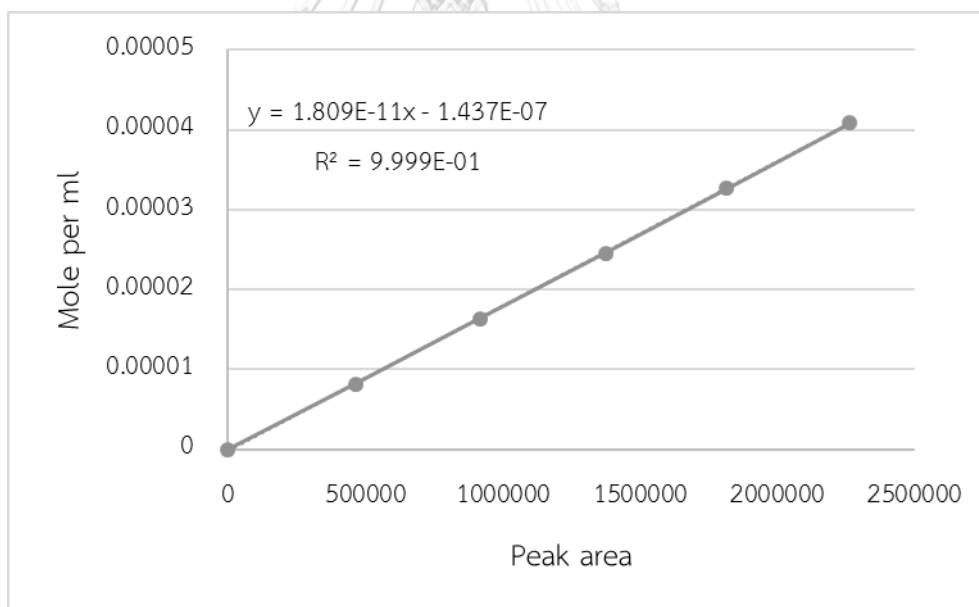
Figure A.3 Calibration curve of O_2
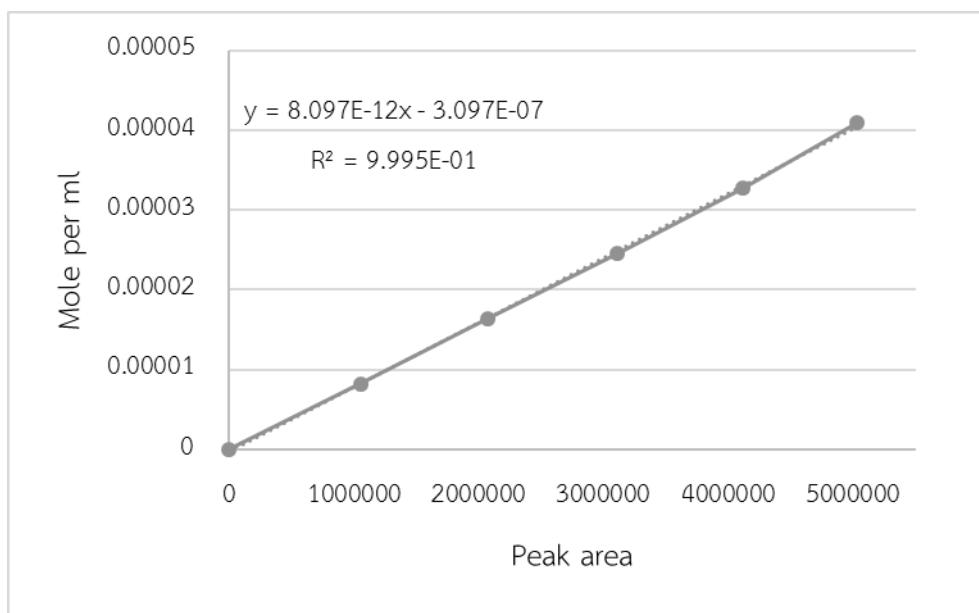
Figure A.4 Calibration curve of CH_4

Text within figure:
y = 8.097E-12x - 3.097E-07
R^2 = 9.995E-01
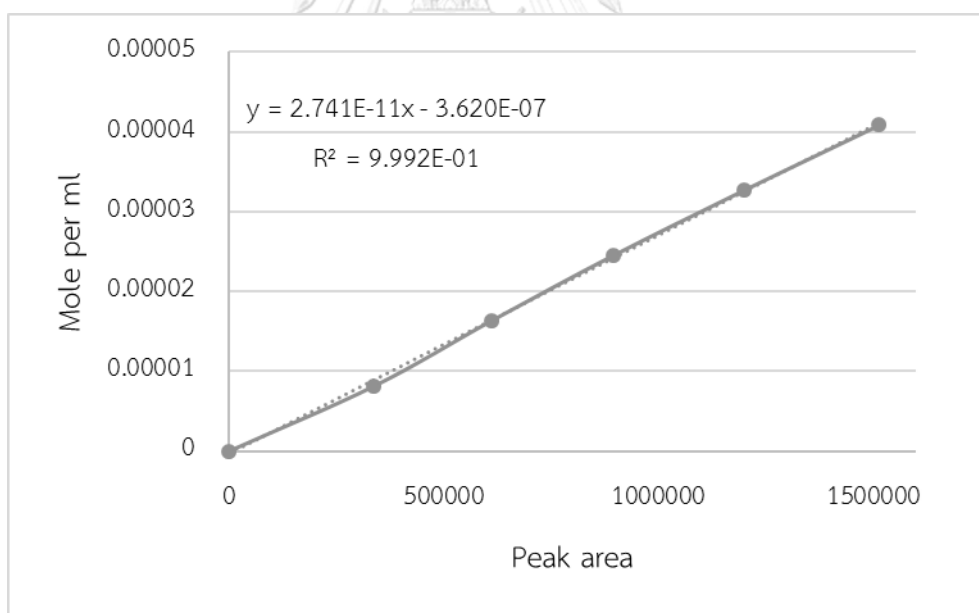
Figure A.5 Calibration curve of CO

Text within figure:
y = 2.741E-11x - 3.620E-07
R^2 = 9.992E-01
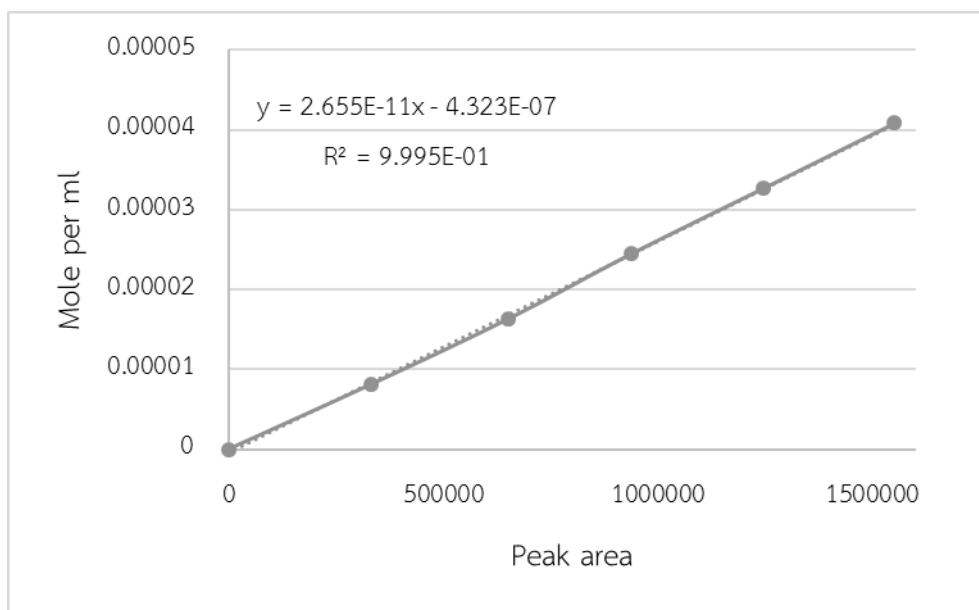
Figure A.6 Calibration curve of CO_2
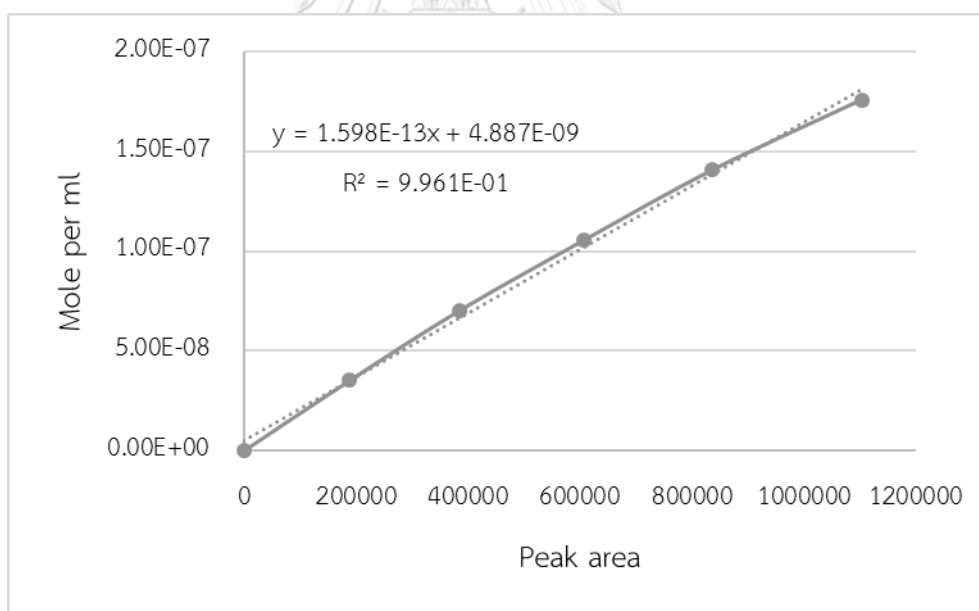
Figure A.7 Calibration curve of C_2H_4O
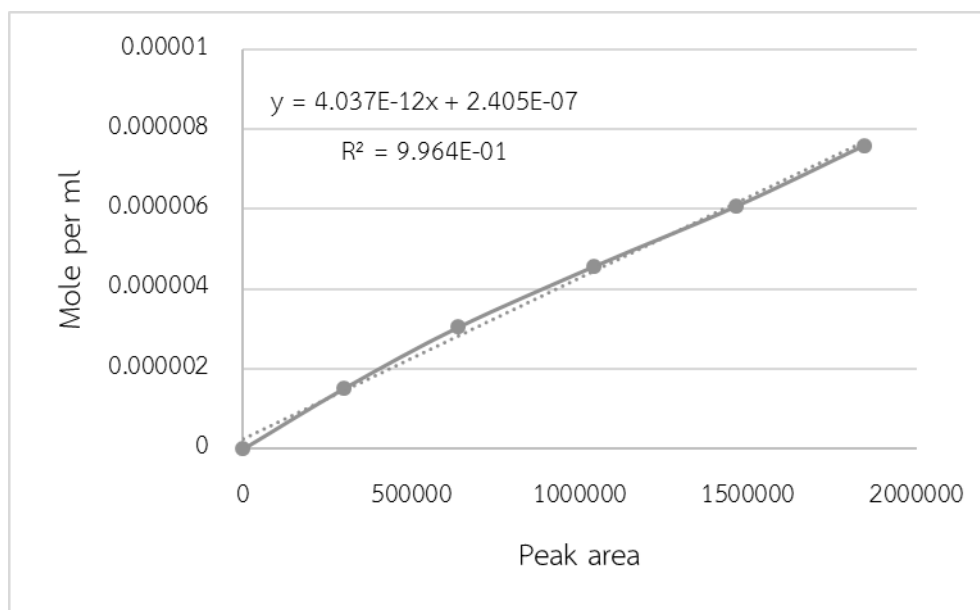
Figure A.8 Calibration curve of C_2H_6O

จุฬาลงกรณ์มหาวิทยาลัย
CHULALONGKORN UNIVERSITY

APPENDIX B

CALCULATIONS

B.1 Oxygen carriers' preparation

N/xLCA oxygen carrier composed of 12.5 wt.% of Ni, x wt.% of La_2O_3, 10-x wt.% of CeO_2 and 77.5 wt.% of Al_2O_3.

The modified support was prepared by wet impregnation method. Alumina and mixed aqueous solution of cerium nitrate hexahydrate ($Ce(NO_3)_3.6H_2O$) and lanthanum nitrate hexahydrate ($La(NO_3)_3.6H_2O$) were stirred at the temperature of 70°C until the solution transforming to slurry. Then, the modified supports were dried and calcined.

$$W_{\text{La precursor}} = W_{\text{Al2O3}} \times \frac{2x}{77.5} \times \frac{MW_{\text{La precursor}}}{MW_{La2O3}}$$

$$W_{\text{Ce precursor}} = W_{\text{Al2O3}} \times \frac{(10-x)}{77.5} \times \frac{MW_{\text{Ce precursor}}}{MW_{CeO2}}$$

Supported Ni oxygen carriers were prepared by wet impregnation method using an aqueous solution of nickel nitrate hexahydrate ($Ni(NO_3)_2.6H_2O$) and using similar procedure as mentioned above.

$$W_{\text{Ni precursor}} = W_{modified\ support} \times \frac{12.5}{87.5} \times \frac{MW_{\text{Ni precursor}}}{MW_{Ni}}$$

where W = Weight, g

MW = Molecular weight, g/mol

B.2 Ratio of lanthanum in Ce-La solid solution

Table B.1 Ratio of Ce and La in oxygen carrier

Oxygen carrier	Rare earth loading (wt.%)		Amount of rare earth (mol/100 g oxygen carrier)		La in solid solution (mol%)
	La_2O_3	CeO_2	La	Ce	La/(La+Ce)
NiO/Al_2O_3	-	-	-	-	-
NiO/CeO_2-Al_2O_3	-	10	-	0.0581	0
$NiO/1La_2O_3$-CeO_2-Al_2O_3	1	9	0.0061	0.0523	10.5
$NiO/3La_2O_3$-CeO_2-Al_2O_3	3	7	0.0184	0.0407	31.2
$NiO/5La_2O_3$-CeO_2-Al_2O_3	5	5	0.0307	0.0290	51.4
$NiO/7La_2O_3$-CeO_2-Al_2O_3	7	3	0.0430	0.0174	71.1
$NiO/9La_2O_3$-CeO_2-Al_2O_3	9	1	0.0552	0.0058	90.5
NiO/La_2O_3-Al_2O_3	10	-	0.0614	-	100

B.3 Sherrers' equation

The crystallite size was calculated from the width at half of height (FWHM) of diffraction peak of the XRD pattern by using Scherrer equation.

$$d = \frac{K\lambda}{Bcos\theta}$$

where d = Crystallite size, A°

K = Crystallite shape factor or Scherrer constant depending on shape of crystal (= 0.9 for FWHM of spherical crystals with cubic symmetry)

B = The width at half of height, radian

λ = X-ray wavelength, (= 1.5418 A° for CuK$_\alpha$)

θ = Observed peak angle, degree

B.4 Basicity

The surface basicity and strength of basic sites for oxygen carriers can be evaluate from the CO_2-TPD profiles by the following steps.

The mole of CO_2 was determined from the calibration curve of CO_2 desorption as following equation:

$$Mole \ of \ CO_2 \ (mmol) \ = \ 0.017624 \times A$$

The number of basic sites of sample was determined by the following equation:

$$The \ basicity \left(\frac{mmol \ CO_2}{g_{oxygen \ carrier}} \right) = \frac{0.017624 \times A}{B}$$

where A = The area of the CO_2-TPD profiles

B = Weight of oxygen carrier, g

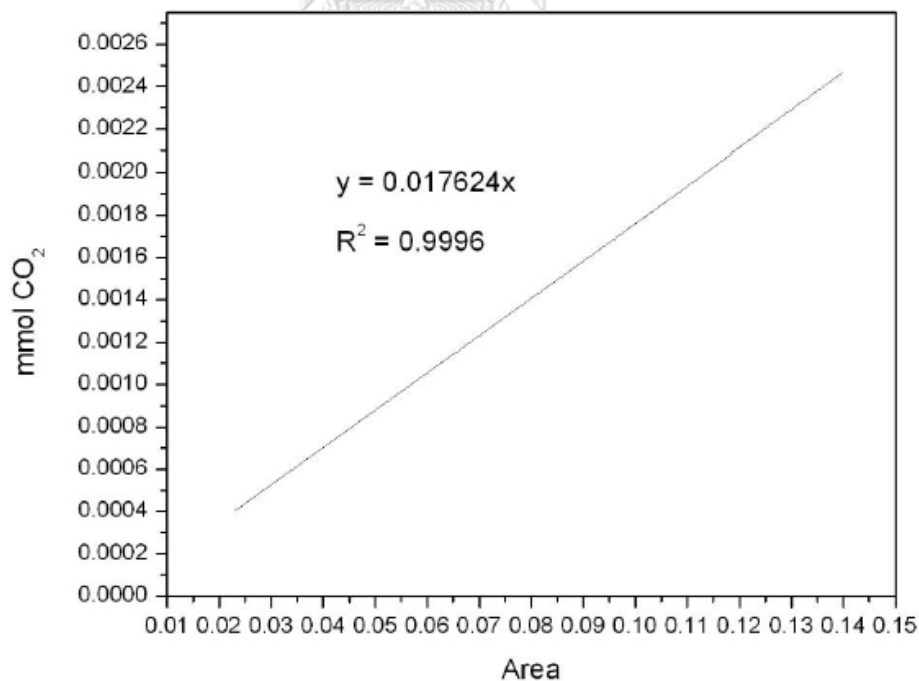**Figure B.1** Calibration curve of CO_2 from CO_2-TPD profiles
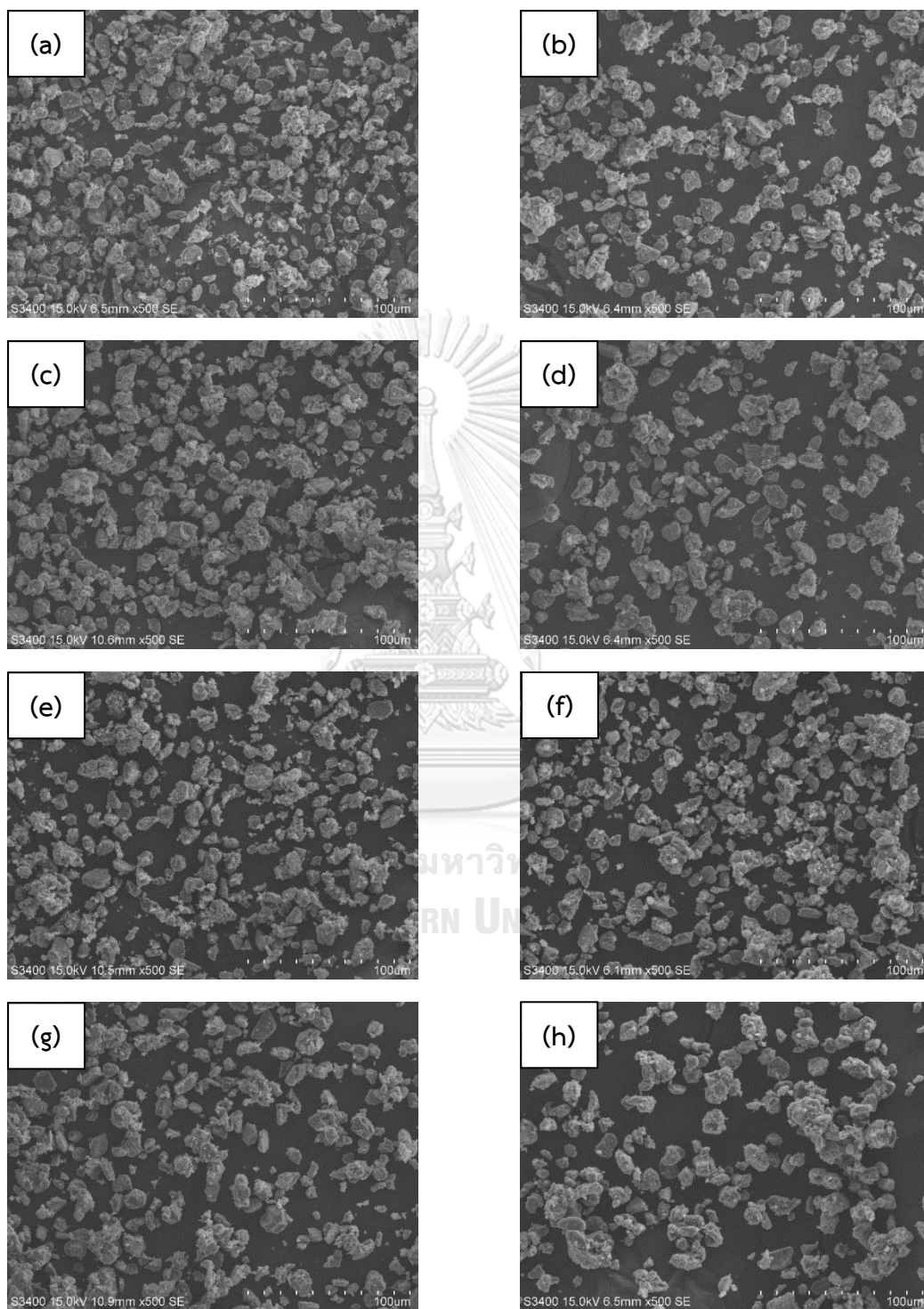
APPENDIX C

SEM-EDX FOR Ce AND La ON OXYGEN CARRIERS

Figure C.1 SEM images of **(a)** N/A **(b)** N/CA **(c)** N/1LCA **(d)** N/3LCA **(e)** N/5LCA **(f)** N/7LCA **(g)** N/9LCA **(h)** N/LA oxygen carrier at 500 magnification
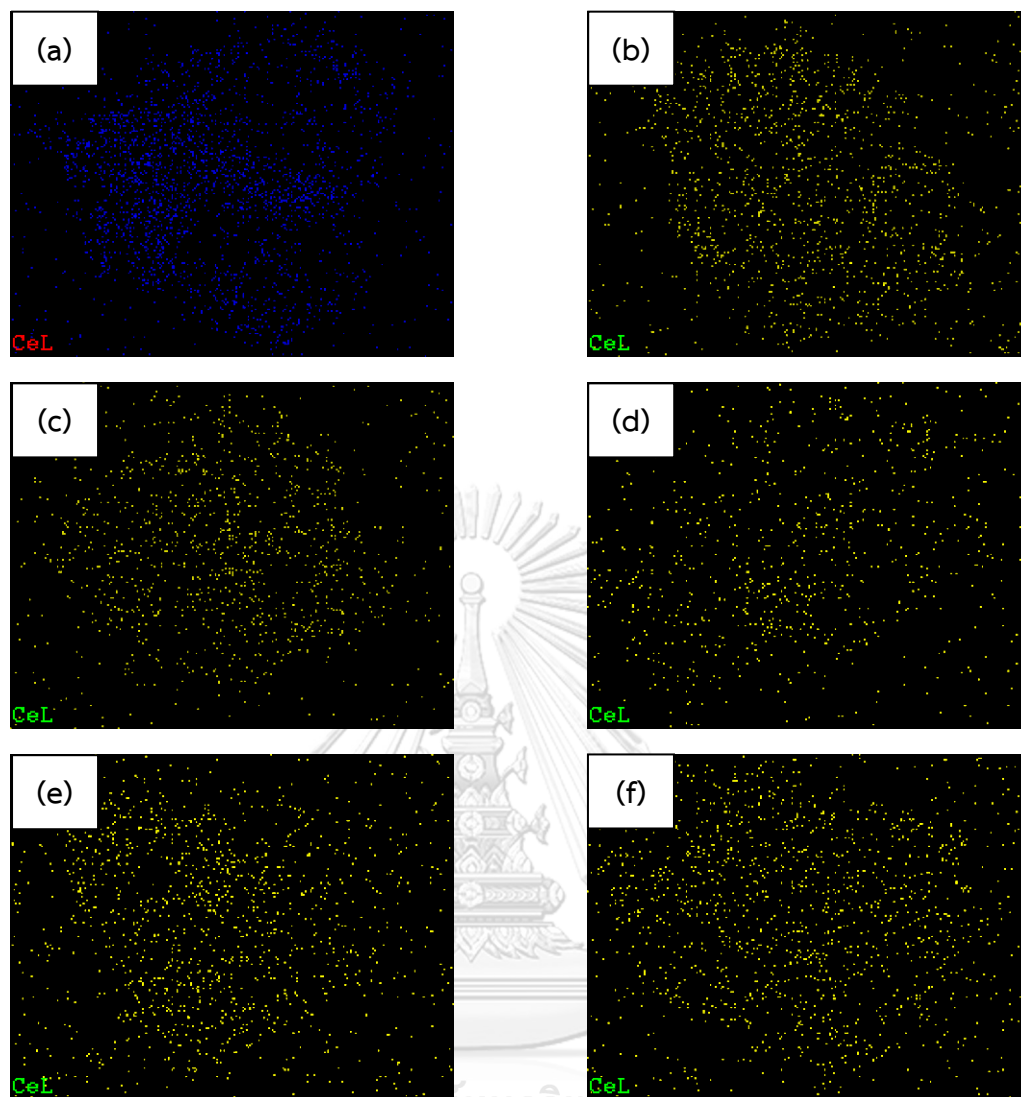
Figure C.2 EDX mapping for Ce on fresh **(a)** N/CA **(b)** N/1LCA **(c)** N/3LCA **(d)** N/5LCA **(e)** N/7LCA **(f)** N/9LCA oxygen carriers
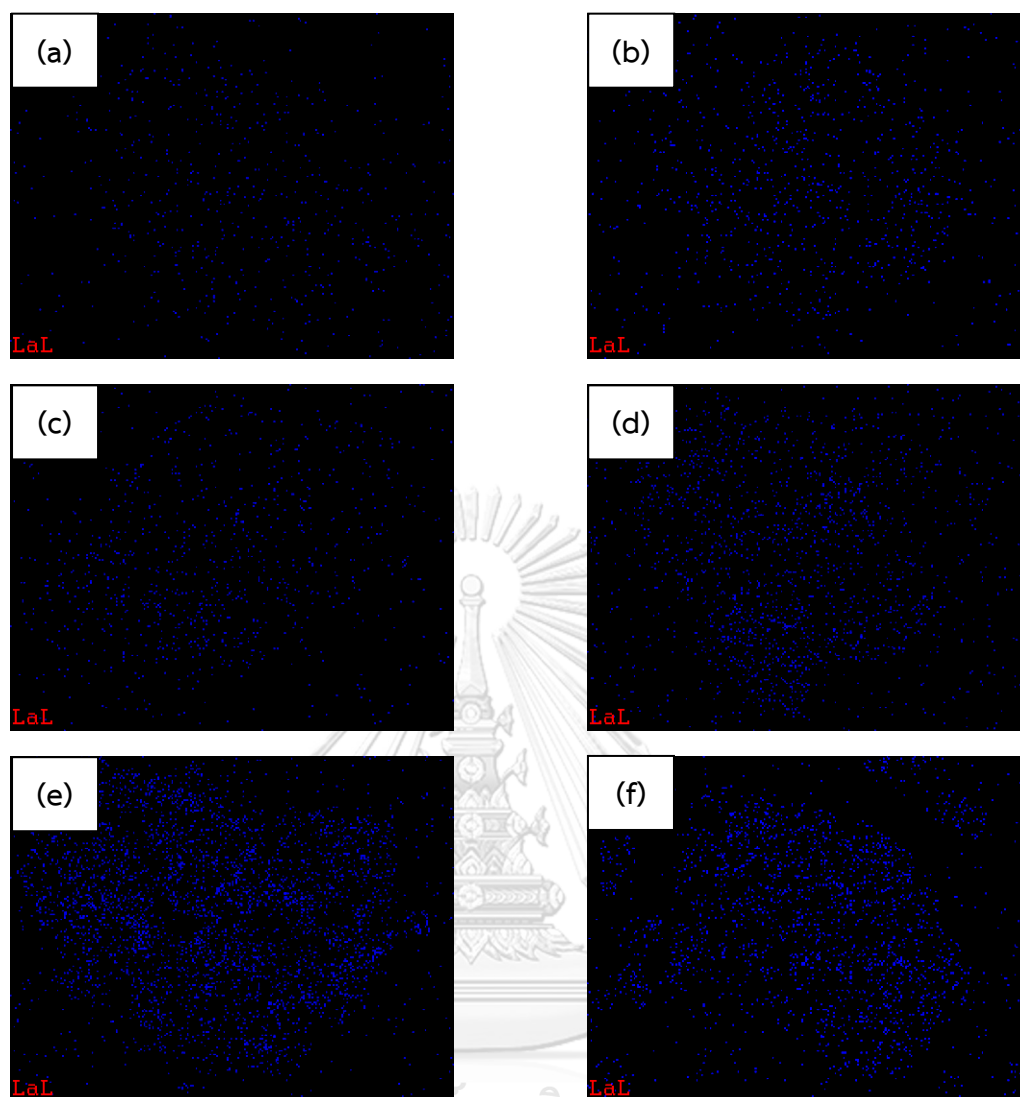
Figure C.3 EDX mapping for La on fresh **(a)** N/1LCA **(b)** N/3LCA **(c)** N/5LCA **(d)** N/7LCA **(e)** N/9LCA **(f)** N/LA oxygen carriers

Table C.1 Element content from EDX mapping of fresh oxygen carriers

Oxygen carrier	Ni (wt.%)	Ce (wt.%)	La (wt.%)
NiO/Al_2O_3	36.81	-	-
$NiO/CeO_2-Al_2O_3$	21.94	16.85	-
$NiO/1La_2O_3-CeO_2-Al_2O_3$	30.03	10.28	1.38
$NiO/3La_2O_3-CeO_2-Al_2O_3$	23.53	9.48	4.48
$NiO/5La_2O_3-CeO_2-Al_2O_3$	21.03	6.31	6.21
$NiO/7La_2O_3-CeO_2-Al_2O_3$	25.77	4.98	9.93
$NiO/9La_2O_3-CeO_2-Al_2O_3$	31.85	2.13	11.26
$NiO/La_2O_3-Al_2O_3$	27.12	-	16.96

VITA

NAME   Supalak Isarapakdeetham

DATE OF BIRTH   20 September 1993

PLACE OF BIRTH   Suphanburi

HOME ADDRESS   90/220 Setthakij Rd., Thasai, Mueng Samutsakhon,

                    Samutsakhon

AWARD RECEIVED   Bachelor degree in Chemical Engineering with first class

                    honours from Mahidol University in 2016